UNIVERSIDAD DE CONCEPCIÓN
FACULTAD DE CIENCIAS FÍSICAS Y MATEMÁTICAS

Origin of supermassive black holes

Predictions from different formation scenarios

Origen de los agujeros negros supermasivos

Predicciones desde distintos escenarios de formación

Profesor Guía: Dr. Dominik Schleicher

Departamento de Astronomía

Facultad de Ciencias Físicas y Matemáticas

Universidad de Concepción

Tesis presentada a la Dirección de Postgrado de la Universidad de Concepción para optar al grado académico de Magíster en Astronomía

---

Matías Andrés Liempi González

Enero 2024

Concepción, Chile

AGRADECIMIENTOS

First of all, I would like to thank the family Liempi-González (including Samy Alberto, Rubia Subercaseaux, Schrodinger, and Hachicko, my pets) who have been part of the entire process of producing this thesis.

I also appreciate the support of all those who have contributed and have been an active part of this thesis with discussions and comments. Among them, especially Dr. Dominik Schleicher, who was always available to discuss not only the project, but also how to make studies compatible with a healthy lifestyle and not being crazy in the process. Without his help and support during the process, it would have been much more difficult to follow through with the project. Also, I appreciate the comments of Dr. Andrés Escala, Dr. Michael Fellhauer and Dr. Andrew Benson, they contributed with useful comments and discussions.

Finally, I would like to mention my friends Juan, Daniela, and Paulina. We shared good moments during the master program talking about life and drinking beer mojitos (and long islands as well).

I would like to appreciate the financial support of the ANID BASAL projects ACE210002 and FB210003, as well as via the Millenium Nucleus NCN19-058 (TITANs).

Resumen

Es posible observar Cúmulos de estrellas Nucleares (CNs) y Agujeros Negros (ANs) en distintas galaxias que pertenecen al universo local. Ambos objetos pueden coexistir o no, pero hay evidencia de que ambos se correlacionan con algunas de las propiedades globales de las galaxias (por ejemplo, el radio del cúmulo y la masa estelar de la galaxia anfitriona o la relación entre el AN central y la velocidad de dispersión del bulbo). La diferencia de ambos objetos radica en su naturaleza, los ANs son los objetos más densos del universo y es imposible obtener una medida directa de sus propiedades. Los CNs son los sistemas estelares más densos observados y, debido a su emisión, es posible obtener más información. La pregunta radica en si estos objectos tienen un origen en común o simplemente es coincidencia que ambos coexistan o tomen el lugar del otro dependiendo del tipo de la galaxia anfitriona.

En esta tesis implementamos un modelo de formación de CNs en Galacticus, un modelo semianalítico para la formación y evolución de galaxias. Nuestro modelo se basa la formación de CNs como resultado de la acumulación de gas en el centro de las galaxias. Además, incluímos un modelo para la formación de semillas de ANs basado en el colapso de estos cúmulos cuando alcanzan una masa crítica. También exploramos como este mecanismo puede afectar la distribución final de la masa ANs. Para ello, ajustamos diferentes parámetros libres en el modelo para reproducir la distribución observada de las masas de los cúmulos nucleares.

Comenzamos con el mejor modelo bariónico de Galacticus, variamos los parámetros relevantes para la evolución de los cúmulos. También exploramos la distribución de las diferentes propiedades de los cúmulos en el momento de colapso para estudiar su impacto.

Nuestro modelo depende fuertemente de la resolución de la simulación, lo cual puede llevar a sobreestimaciones y subestimaciones en la población de los CNs predicha por los distintos modelos. El colapso de los cúmulos se ve fuertemente favorecido cuando consideramos un porcentaje menor del radio para el cálculo de la masa crítica, aún así la población de ANs permanece subestimada para los más masivos, indicando que hay más escenarios de formación por investigar.

Keywords – Agujeros negros, galaxias: núcleo, métodos: analítico

Abstract

It is possible to observe Nuclear Stars Clusters (NSCs) and Black Holes (BHs) in different galaxies observed in the Local Universe. Both objects may or may not coexist. But there is evidence that both are correlated with some of the global properties of galaxies (for example, cluster radius and stellar mass of the host galaxy or the correlation between the central BH and the velocity dispersion of the bulge). The difference between both objects lies in their nature, BHs are the densest objects in the Universe and it its impossible to obtain a direct measurement of their properties while NSCs are the densest star systems observed and, due to their emission, it is possible get more information. The question is whether these objects have a common origin or is it simply a coincidence that both coexist or take the place of the other depending on the type of the host galaxy.

In this thesis, we implement a model of NSC formation in Galacticus, a semi-analytical model for the formation and evolution of galaxies. Our model is based on the formation of NSCs as a result of the accumulation of gas in the center of galaxies. Additionally, we include a model for the formation of BH seeds based on the collapse of these clusters when they reach a critical mass. We also explore how this mechanism can affect the final distribution of black hole mass. To do this, we adjust the different free parameters in the model to reproduce the observed mass function of the NSCs.

We start with the best baryon model of Galacticus and vary the relevant parameters for the evolution of the NSCs. We also explore the distribution of the different properties of the NSCs at the moment of collapse to study its impact.

Our model is strongly dependent on the resolution of the simulation, which can lead to overestimations and underestimates in the NSC population predicted by the different models. The collapse of the NSCs is strongly favored when we consider a smaller percentage of the radius for the calculation of the critical mass, but the population of BHs still remains underestimated for the most massive, indicating that there are more formation scenarios to investigate.

Keywords – black hole physics, galaxies: nuclei, methods: analytical

Contents

List of Tables

List of Figures

Chapter 1

Introduction

Black Holes (BHs) are one of the most interesting objects in the Universe. It being difficult to directly measure their observables, such as mass, charge, and spin, it makes it difficult to build theoretical models to understand the conditions under which they form, growth, and how they are related to the evolution of galaxies.

The nature of BHs is still unclear; From observations we identify mainly two families of astrophysical BHs (Volonteri, 2010), and the classification is based on their mass.

Stellar BHs come from the end of stellar evolution, with masses in the order of $\sim 10\ M_{\odot}$. However, the collapse of zero-metallicity stars leads to several hundred solar mass BHs (Bond et al., 1984; Fryer et al., 2001; Heger et al., 2003). On the other hand, the Supermassive Black Hole (SMBH) term refers to a BH at the center of a galaxy with masses up to and above several billion solar masses (Volonteri, 2010).

We know of the existence of very massive objects of masses $\sim 10^6 - 10^9\ M_{\odot}$ in the nucleus of galaxies from the last century (Zel'dovich, 1964; Salpeter, 1964; Ghez et al., 2008; Gillessen et al., 2009; Moran et al., 2014), which were later known as SMBHs. Recently, we have evidence of the existence of another type of dense object detected in the nucleus of galaxies, called Nuclear Star Clusters (NSCs). NSCs are considered to be the densest stellar configuration in the Local Universe (Böker et al., 2004; Côté et al., 2006; Walcher et al., 2006; Balcells et al., 2007; Hoyer et al., 2021).

Both objects seem to be correlated with different properties of their host galaxies. Furthermore, it is possible to observe both objects coexisting in the center of galaxies and also cases in which only one object is present depending on the stellar mass of the galaxy.

The aim of this thesis is to study the formation of SMBH seeds in NSCs and its impact on the SMBH population. For this purpose, in Section 1.1 we discuss our current knowledge of SMBHs and, similarly, in Section 1.2 for NSCs. Finally, in Section 1.3 we review the observed coexistence of both objects at the center of galaxies.

1.1 Supermassive black holes

Recent observations confirming the presence of SMBHs at the center of galaxies in the local universe have significantly advanced our understanding of the physics close to these objects. Two examples are the direct observation of the shadow of M87* (Event Horizon Telescope Collaboration et al., 2019) and, recently, the observation of the shadow of the SMBH located at the center of the Milky Way, Sag A* (see Fig. 1.1.1).

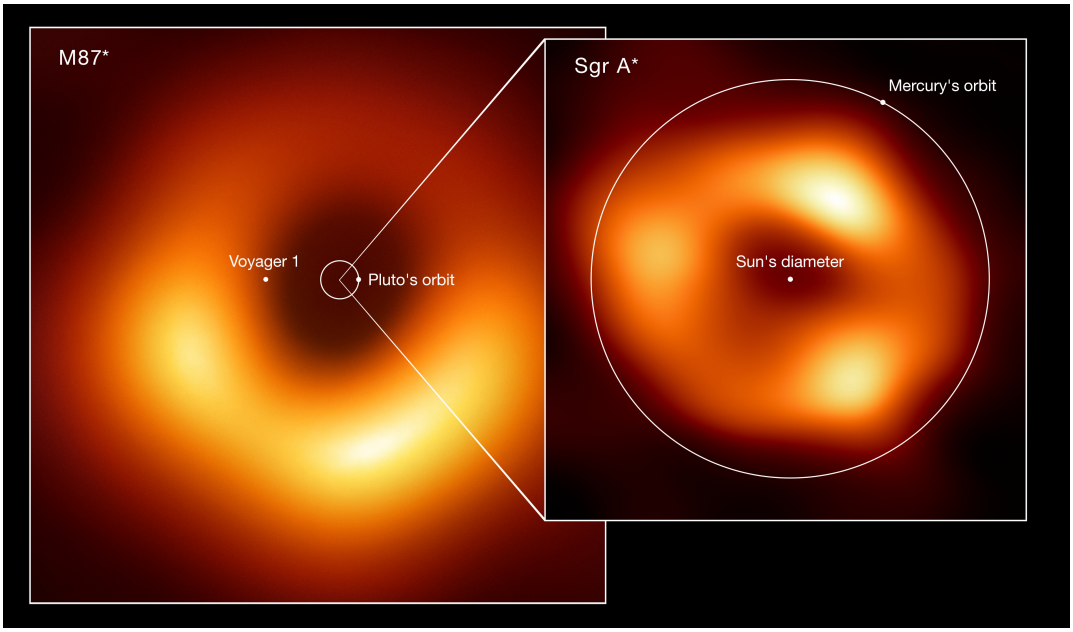

Figure 1.1.1: Size comparison of the two black holes imaged by the Event Horizon Telescope (EHT) Collaboration: M87* (Event Horizon Telescope Collaboration et al., 2019) and Sgr A* (Event Horizon Telescope Collaboration et al., 2022). The image shows the scale of Sgr A* compared to M87* and the orbits of Pluto and Mercury. The diameter of the Sun and the current location of the Voyager 1 space probe, the farthest spacecraft from Earth is also displayed.

Source: EHT collaboration.

These findings prompt us to inquire whether the occurrence of SMBHs in galactic centers is exclusive to our Local Universe or extend beyond it.

Furthermore, we observe correlations between the mass of the SMBH and the different properties of their host galaxies (Ferrarese and Merritt, 2000; Tremaine et al., 2002). The most known correlation is between the mass of the SMBH and the stellar velocity dispersion of the bulge of the host galaxy,

$$\frac{M_\bullet}{10^9\ M_\odot} = (0.30^{+0.037}_{-0.033}) \left(\frac{\sigma}{200\,\mathrm{km\,s^{-1}}}\right), \tag{1.1.1}$$

where $M_\bullet$ is the mass of the BH and σ is the dispersion velocity of the bulge of the galaxy. More correlations (and their implications) are reviewed and discussed in Kormendy and Ho (2013). The existence of different correlations allows us to wonder whether the formation of galaxies is linked (or not) to the formation of

SMBHs. To answer this question, we must look to the past, specifically, to the first black holes detected.

1.1.1 The first black holes

The most reliable observational support for the existence of SMBHs in the Early Universe comes from the observation of high redshift quasars.

There are three different critical spatial scales (Fan et al., 2023) to describe the mechanisms responsible for feeding the quasar. Of those three scales, two are directly related to SMBHs:

- At distances less than 1 pc of the center of the galaxy, the mechanism responsible of the quasar emission is from well within the SMBH sphere of influence.
- At larger distances $\sim 1 - 10$ kpc, the evolution of quasars and galaxies is strongly coupled. An example is the correlation between the mass of the SMBH and the velocity dispersion of their host galaxies (see Equation 1.1.1).

It is possible to find different observations of quasars at redshifts up to $z > 7$. A catalog with more than 100 quasars is available in Bañados et al. (2016), with samples at $5.6 \lesssim z \lesssim 6.7$, which means that SMBHs had up to ~ 1 Gyr to grow and reach masses of about $\sim 10^6 - 10^{10}\ M_\odot$ (Natarajan and Treister, 2009; Volonteri, 2010; King, 2015; Pacucci et al., 2017). Figure 1.1.2 shows the mass of BHs versus the age of the Universe and shows how different formation scenarios cannot explain masses higher than $10^6\ M_\odot$.

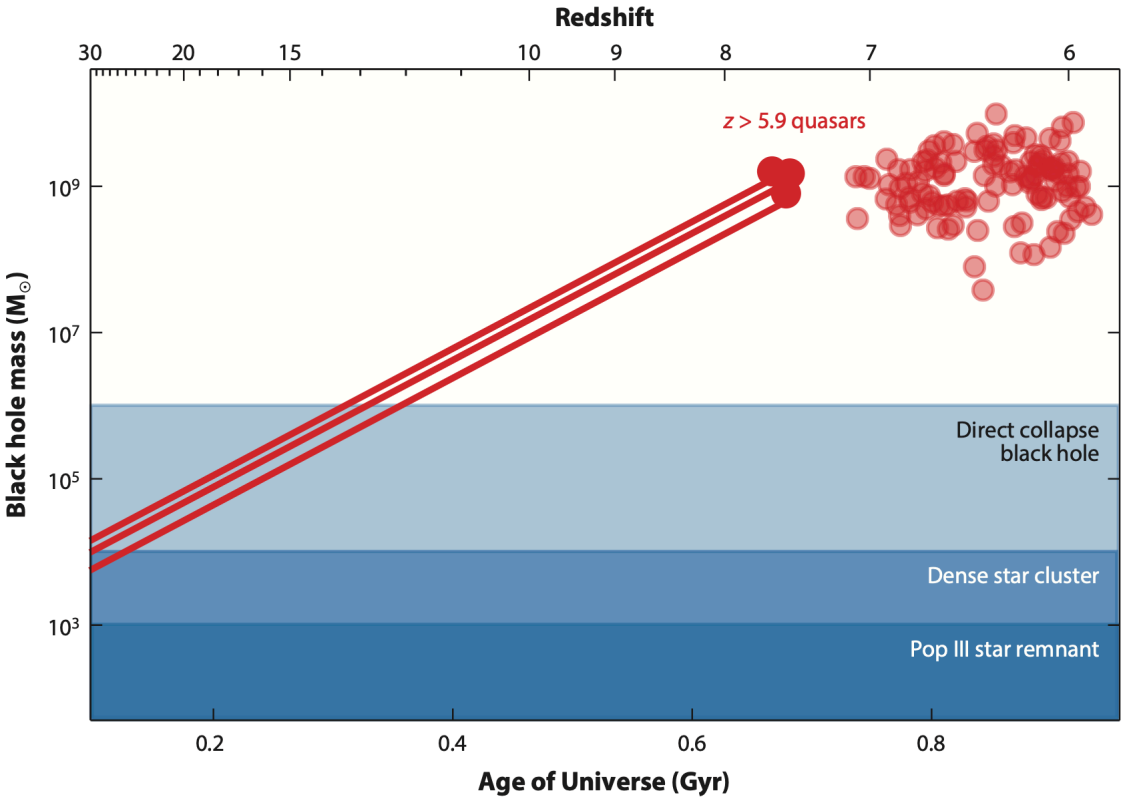

Figure 1.1.2: BH mass versus age of the Universe (and redshift). The red circles mark the compilation of robust M_{gII} SMBH masses for quasars at $z > 5.9$. The red lines show the growth history (assuming constant, maximum Eddington-limited accretion) of the most distant quasars at $z > 7.5$. The shaded regions represent the mass ranges for popular BH seed formation scenarios.

Source: Fan et al. (2023)

Surprisingly, there are candidates for quasars up to $z = 12$ using data from the Prime Extragalactic Areas for Reionization Science (PEARLS) survey and the Early Release Observations (ERO) from the James Webb Space Telescope (Juodžbalis et al., 2023). If these candidates are confirmed, the SMBHs would have ~ 0.4 Gyr to reach higher masses.

In summary, we know where to find SMBHs. It is possible to find them in almost all centers of galaxies, observing quasars at different redshifts. However, how they reach larger masses is still unclear, and the simple answer is that they must grow on short timescales (Inayoshi et al., 2020), opening the possibility for new formation scenarios.

1.1.2 Formation of supermassive black holes

Different mechanisms have been proposed to explain the formation of SMBHs (Rees, 1984; Volonteri, 2010; Woods et al., 2019; Inayoshi et al., 2020). Although formation can occur in different contexts; in essence, they can be summarized in one simple idea.

All systems that depend on the gravitational potential undergo a runaway process because the potential gets deeper and deeper, being inevitable that a large fraction of the dense object mass collapses into a SMBH seed (Rees, 1984). We refer to a seed as a BH of an unconstrained initial mass. The range of masses is from $\sim 10^2\ M_\odot$ to $\sim 10^5\ M_\odot$ (Volonteri, 2010).

Using this scheme, we can explain the formation of SMBHs from the Direct Collapse (DC) of a massive gas cloud ($\sim 10^6 - 10^8\ M_\odot$) when the cooling process is suppressed during collapse. This mechanism can form seeds of the order of $\sim 10^5\ M_\odot$ (Rees, 1984; Volonteri and Rees, 2005; Ferrara et al., 2014; Latif and Schleicher, 2015; Regan and Downes, 2018).

Another plausible mechanism is the collapse of remnants of Population III (Pop. III) stars (Haiman, 2004; Whalen and Fryer, 2012; Latif et al., 2013; Singh et al., 2023). These stars, formed from zero-metallicity gas in minihalos of mass $\approx 10^6\ M_\odot$ (Volonteri, 2010), are expected to have stellar masses ranging from $\sim 10\ M_\odot$ to $\sim 10^2\ M_\odot$ (Hirano et al., 2014, 2015). The mass of the formed seed is strongly dependent on the mass of its progenitor. For low-metallicity stars ($25 - 140\ M_\odot$) the mass of the formed remnant is close to the half-mass of the progenitor (Zhang et al., 2008). If there is a light BH seed that is forming, it is not relevant to the system because of its similar mass to that of the companion stars.

In Pop. III stars with masses between $140 - 260\ M_\odot$, the collapse is reserved due to the domain of pair instability supernovae. This prevents the collapse, and the star contracts rapidly until it is able to burn oxygen and silicon. Finally, these stars are completely disrupted by the nuclear explosion. The core implodes, burns fuel, and explodes, leaving no remnants (Kudritzki and Puls, 2000; Fryer et al., 2001).

Finally, the most massive Pop. III stars (masses over $260\ M_\odot$ during their main-

sequence lifetime), the photodisintegration instability occurs before explosive burning reverses the implosion (Bond et al., 1984). The nuclear energy generated by pairs is not sufficient to prevent the implosion forming a massive BH (Fryer et al., 2001).

1.2 Nuclear star clusters

In recent years, our knowledge of NSCs has advanced rapidly because of the improvement on the resolution of telescopes. Recent observational and theoretical work suggests that many NSC properties, such as the stellar bulge and/or the central supermassive black hole, scale with properties of their host galaxies (e.g., Ferrarese et al., 2006; Wehner and Harris, 2006; Li et al., 2007; Graham and Spitler, 2009; Genzel et al., 2010; Leigh et al., 2012; Antonini et al., 2015).

NSCs are extremely dense and massive star clusters that occupy the innermost region or nucleus of most galaxies (Böker et al., 2002; Côté et al., 2006; Neumayer et al., 2020). Their presence is independent of the morphological type of the host galaxy (Light et al., 1974). For example, the work of Lyubenova et al. (2013) demonstrates the existence of a NSC in FCC 277, a nucleated elliptical galaxy in the Fornax cluster, while early observations of nearby galaxies such as M 31, an Sb galaxy (Redman and Shirley, 1937), or M 33, an Sc galaxy (Mayall and Aller, 1942), reveal prominent and compact surface brightness peaks in the center of the host galaxy, which were confirmed as a result of the presence of NSCs (Milosavljević, 2004; Eckner et al., 2018).

Even though NSCs are present in different types of galaxies, recent investigations show that scaling properties between NSCs and their hosts galaxies are different in early- and late-type galaxies. The study of Georgiev et al. (2016) explores the scaling relations between the NSC mass and the total stellar mass of the host galaxy using a large sample of NSCs. The parameters for the fitted relations of NSC and its host galaxies are different depending on the type of host galaxy. The relation between the effective radius of the NSC and the stellar mass of the host in late-type galaxies is

$$\log\left(\frac{r_{\rm eff,NSC}}{3.44\ \rm pc}\right) = 0.356^{+0.056}_{-0.057}\log\left(\frac{M_{\star,\rm gal}}{5.61\cdot 10^{9}\ M_{\odot}}\right) - 0.012^{+0.026}_{-0.024}, \qquad (1.2.1)$$

where $M_{\star,\mathrm{gal}}$ is the stellar mass of the galaxy and r_{eff} is the effective radius of the NSC. For early-type galaxies, the relation is given by

$$\log\left(\frac{r_{\mathrm{eff,NSC}}}{6.11\ \mathrm{pc}}\right) = 0.326^{+0.055}_{-0.051}\log\left(\frac{M_{\star,\mathrm{gal}}}{2.09\cdot 10^{9}\ M_{\odot}}\right) - 0.011^{+0.015}_{-0.011}. \tag{1.2.2}$$

A possible explanation for the difference in these relations could be the existence of different pathways to form NSCs in different galaxies.

1.2.1 Formation of nuclear star clusters

Our current models of NSC formation and evolution are based primarily on two scenarios: a globular cluster migration channel and an in situ star formation channel at the center of the host galaxy. More theoretical scenarios proposed; nevertheless, we focus on the most observationally supported scenarios.

1.2.1.1 Globular cluster migration

As NSCs have been observed in different types of galaxies, it is natural to investigate the conditions under which NSCs form. There is no simple model, but one of the first studies suggests that NSCs may form through the infall and merging of globular clusters driven into the nucleus by dynamical friction (Tremaine et al., 1975). Following this scheme, different analytic works made by Capuzzo-Dolcetta (1993) and Lotz et al. (2001) explored this scenario obtaining similar conclusions. However, the best proof for this mechanism was performed a year earlier by Oh and Lin (2000) with N-body simulations.

The physical process is governed by dynamical friction within the host galaxy stellar body, causing globular clusters to be gradually pulled toward the nucleus during their orbital motion. Of course, the strength of the dynamical friction depends on the mass of the cluster and the velocity of the stars in the host galaxy, which results in shorter (or larger) timescales to reach the center of the galaxy.

Different observations show in the inner region of early-type galaxies, close to the nucleus, that there is no evidence of the presence of massive globular clusters (Lotz et al., 2001; Capuzzo-Dolcetta and Mastrobuono-Battisti, 2009), supporting the validity of the mechanism and also explaining the existence of a metal-poor

stellar population in the center of galaxies.

Many numerical and semi-analytic models quantify the efficiency of dynamical friction. These results can be summarized as in host galaxies with early star formation, the number of high-mass clusters (stellar masses above 10^5 $M_\star$) is sufficient to be a plausible mechanism to form an NSC on time scales shorter than Hubble time (e.g., Capuzzo-Dolcetta, 1993; Oh and Lin, 2000; Lotz et al., 2001; Agarwal and Milosavljević, 2011; Neumayer et al., 2011). As mentioned before, the time scale plays an important role in this scenario. The work by Milosavljević (2004) demonstrates that this mechanism fails in pure disk galaxies as a result of the migration time scales being too long. In consequence, another possible scenario is suggested in the same article, where gas infall and subsequent in situ star formation were the more plausible alternative in disk galaxies.

1.2.1.2 In situ star formation in the galactic nucleus

As mentioned in Section 1.2.1.1, due to the large time scale for the migration of globular clusters to the centers in disk-like galaxies, another scenario should explain the existence of NSCs in late-type galaxies.

In this scenario, it is suggested that in situ star formation occurs when the gas reaches the central few pc and triggers an intense burst of star formation (Milosavljević, 2004).

There are different mechanisms proposed to be responsible for the gas transference and accumulation in the galactic nuclei, to be available for star formation.

The first reasonable mechanism is a bar-driven gas infall, where the gas will move inward as a response of a non-axisymmetric potential (Shlosman et al., 1990). Gas movement can occur through regular flows in nuclear spirals and/or due to loss of angular momentum in star formation rings caused by dynamical resonances (e.g., Maciejewski, 2004; Kim and Elmegreen, 2017; Hunt et al., 2008). The observations of NGC 6946 show a clear example of this process, where the estimation of the molecular gas mass is up to 6×10^7 $M_\odot$ within a radius of 30 pc that feeds the growth of the NSC (Schinnerer et al., 2006, 2007). In the same way, there are simulations that suggest the fuelling of central regions is an active process in the local Universe, at least in systems like NGC 6946 (Emsellem et al., 2015).

Another plausible explanation is the dissipative nucleation that occurs at high redshift. In this process, there is clumpy star formation in nuclear spirals, which will infall and merge in the center of the galaxy. This explains the nucleation of spheroidal galaxies that are now devoid of gas (Bekki et al., 2006; Bekki, 2007), and the low nucleation rate in the least massive galaxies is a consequence of the feedback from stellar winds, and supernova explosions will more easily expel the gas before it reaches the center of the galaxy.

In galaxies with Sérsic index less than 3.5 (a flat density profile) and, in the absence of a NSC, the tidal forces act on the gas within about 0.1% of the effective radius of the galaxy, compressing the gas and forming the NSC. This mechanism can explain the observed scaling between the mass of the NSC and the host spheroid (Emsellem and Van De Ven, 2008).

Finally, the magneto-rotational instability is also studied as a mechanism for the radial gas transport towards the nucleus. A diffentially rotating disk of gas under the influence of a weak magnetic field will lead to the magneto-rotational instability causing the gas mass transference, reaching NSC stellar masses in the order of 10^6 $M_\odot$ in ~ 1 Gyr (Milosavljević, 2004).

1.3 Nuclear star clusters and supermassive black holes

We have direct evidence of NSCs dominating the center of galaxies with stellar masses in the range $\sim 10^8 - 10^{10}$ $M_\odot$ (Neumayer et al., 2020). In more massive galaxies, we find SMBHs placed in the center (Kormendy and Ho, 2013). Even so, there are different observations of both objects coexisting in the center of galaxies (Filippenko and Ho, 2003; Seth et al., 2008; Graham and Spitler, 2009; Neumayer et al., 2011; Civano et al., 2012; Nguyen et al., 2019).

As mentioned in Section 1.1.2, different pathways have been proposed to explain the formation of SMBHs in different environments. One interesting channel is the formation through runaway collisions of BHs within dense (nuclear) star clusters (e.g., Portegies Zwart and McMillan, 2002).

1.3.1 Collisions in nuclear star clusters

There are different studies exploring star collisions in NSCs. An example is the work of Sanders (1970), where the effects of stellar collisions, such as mass and energy losses, are investigated by numerical calculations in a simulation of dense stellar systems. In the same way, Lee (1993) studies the dynamical evolution of dense clusters of compact stars using direct N-body simulations. He finds that a SMBH seed can be formed by runaway growth in a dense cluster of compact stars, and the possibility of runaway growth in dense clusters of normal stars is open.

In recent years different numerical simulations have supported the formation of massive objects in the center of stellar clusters due to runaway collisions of massive stars (Miller and Hamilton, 2002; Reinoso et al., 2018, 2020; Vergara et al., 2023).

In this context, Escala (2021) proposes that the observed NSCs are in a regime where collisions are not relevant throughout the entire system, whereas well-resolved observed SMBHs are found in regimes where collisions are expected to be dynamically relevant (see Figure 1.3.1).

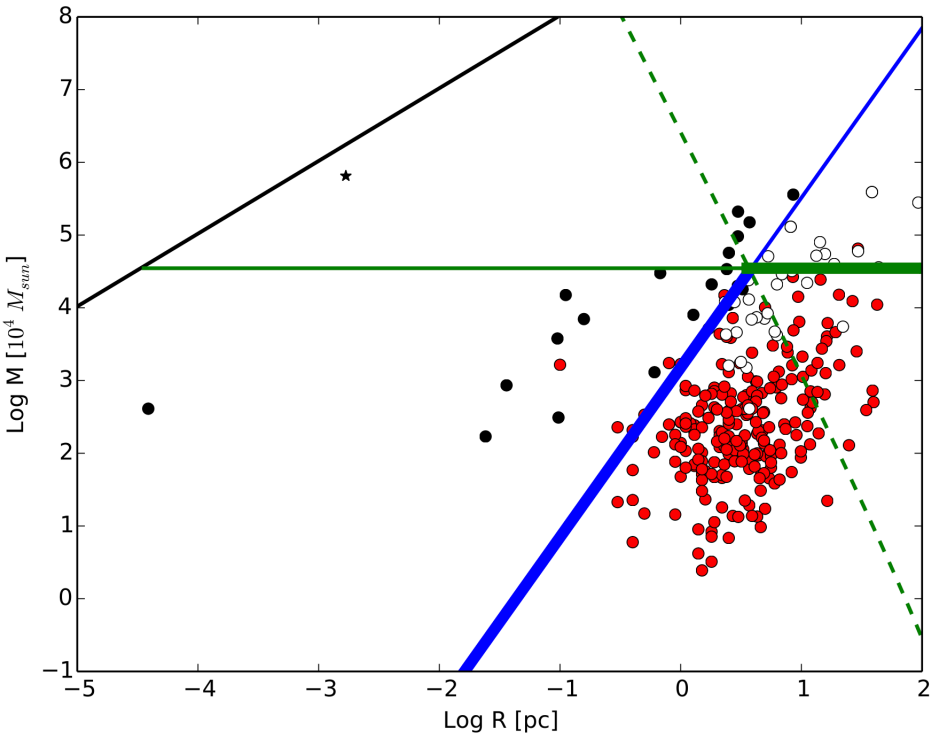

Figure 1.3.1: The positions of NSCs are restricted within the boundaries defined by the collisional stable region for NSCs, denoted by the thicker blue and green lines. The blue line denotes the condition that the characteristic age of the system is comparable or longer than the collision time: $t_{\rm coll} < t_{\rm H}$. The solid green line denotes the intersection between the relaxation time (dashed green line) and the collision time combined with the empirical relation between the NSC mass and the velocity dispersion

Source: Escala (2021)

Following this scheme, the results of Vergara et al. (2023) show that in NSCs with masses larger than a critical mass, collisions become very relevant and form a massive object (Vergara et al., 2023). In Figure 1.3.2, it is possible to observe a trend in the efficiency of the massive object formed and the initial mass of the NSC normalized by the critical mass. We talk in more detail about this critical mass in Section 4.2.

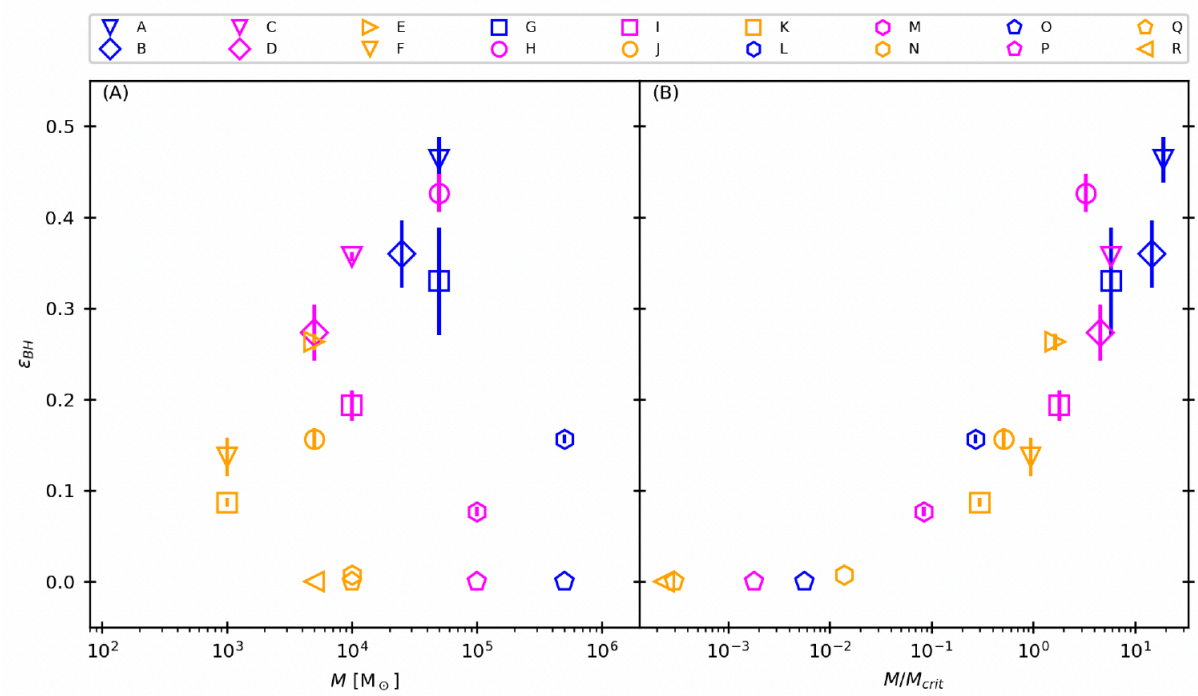

Figure 1.3.2: The left panel (A) of Fig. 5 is the black hole formation efficiency computed by $\epsilon_{\rm BH} = (1+\frac{M_{\rm NSC}}{M_{\rm BH}})^{-1}$ for 10 Myr against the initial mass of the nuclear star cluster. The right panel (B) of Fig. 5 is the black hole formation efficiency computed against the initial mass of the nuclear star cluster normalized by the critical mass

Source: Vergara et al. (2023)

The aim of this thesis is to implement a NSC formation and evolution and a collapse model to form BH seeds based on the critical mass criterion.

In Chapter 2 we briefly review the current galaxy formation theory and the computational methods used to model it. In Chapter 3 we describe the main concepts for modifying Galacticus and some functionalities. The physics of the model that we include is described in 4, while the setup is in Chapter 5. Finally, the details of the simulations and their results are disscused in Chapter 6 and the conclusion and future work are in Chapter 7.

Chapter 2

Galaxy formation theory

In this chapter we introduce how cosmological simulations of galaxy formation and evolution work. For this purpose, we overview the key aspects of galaxy formation theory and the current techniques for computational simulations.

For a long time, galaxy formation and evolution have been central topics in modern cosmology. The importance of their study begins with the first confirmation of galaxies as extra galactic objects (Hubble, 1929).

Today we know the process of galaxy formation involves non-linear physics and a wide variety of physical processes making it impossible to use full analytic models. In that way, the theory is usually split into two parts:

- First, modelling the formation and evolution of the Dark Matter (DM) halos distribution hosting galaxies using N-body simulations or analytical methods (e.g, Press-Schechter theory).
- Then, we model the evolution of baryonic matter distributed in DM halos formed in the previous step (Cora, 2013).

The modern theory of galaxy formation is set within the larger-scale $\Lambda-$Cold Dark Matter (ΛCDM) cosmological model (Blumenthal et al., 1984; Narlikar and Padmanabhan, 2001; Frenk, 2002; Bertone et al., 2005). This model can well explain the Cosmic Microwave Background (CMB) (Komatsu et al., 2009) and the large-scale structure (Seljak et al., 2005; Percival et al., 2007a; Ferramacho et al., 2009; Sánchez et al., 2009). However, galaxy formation occurs at scales much smaller than the CDM and we cannot fully rule out the possibility that

DM is warm or self-interacting.

The key physical processes involved in galaxy formation and evolution are gravity, cooling, star formation, feedback, mergers, and chemical evolution.

2.1 Cosmology

Different experiments measured the CMB (Dunkley et al., 2009), large-scale structure (Tegmark et al., 2004; Percival et al., 2007a,b), Type Ia supernova magnitude redshift (Riess et al., 2018), have shown strong constraints on the determination of the parameters of the ΛCDM cosmology.

From observations (Komatsu et al., 2011) we know that our Universe is one in which the energy density is shared between dark energy ($\Omega_\Lambda = 0.726^{+0.015}_{-0.016}$), dark matter ($\Omega_c = 0.227 \pm 0.014$) and baryonic matter ($\Omega_b = 0.0456 \pm 0.0016$), with a Hubble parameter of $70.4^{+1.3}_{-1.4}$ km/sMpc. Perturbations in the uniform model seem to be well described by a scale-free primordial power spectrum with power law index $n_s = 0.963 \pm 0.012$ and amplitude $\sigma_8 = 0.809 \pm 0.024$.

With this model, we estimate that the age of the universe is about 13.75±0.11Gyr old. In this context, galaxies probably began forming at $z \sim 20 - 50$ (Tegmark et al., 1997; Gao et al., 2007).

2.2 Structure Formation

In any cosmology, after fixing the initial conditions, gravity determines the shape and amplitude of the primordial power spectrum of density fluctuation. The final result of the non-linear evolution of a DM density perturbation is the formation of a DM halo. These DM haloes grow through mergers. This is known as hierarchical structure formation. The recorded evolution of these DM halos mergers is called merger trees (see Figure 3.0.1 for a visual representation).

It is easy to think of DM halos as a construction block. The blocks used to build a final DM halo are called progenitors, and the reconstruction of the history is the merger tree. In those merger trees, DM halos have over-densities in which gas falls and cools down and eventually forms galaxies (Neistein and Dekel, 2008).

The observed and predicted DM halos with N-body simulations (e.g. Klypin

and Shandarin, 1983; Springel et al., 2005b; Heitmann et al., 2010) show that a network of DM halos strung along walls and filaments. This is consistent with measurements of galaxy and quasar clustering on a wide range of scales.

2.3 Halo properties and distribution

It is important to study the properties of the halos. They are the result of the nonlinear evolution of a DM density perturbation and are approximately stable, near-equilibrium state supported against its own self-gravity by the random motions of its constituent particles. This is the formation of the first generation of DM halos. As we assume a hierarchical Universe, the first halos are the progenitors of the later generation of DM halos that form from the merging of these earlier generations of halos.

That is why it is important to study the distribution of their masses at any redshift and the distribution of their formation histories (i.e., have all halos with a given mass M formed in the same way?).

To answer this question, the formalism introduced by Press and Schechter (1974) associates halos with peaks in the Gaussian random density field of DM in the Early Universe.

This formalism allows us to estimate the distribution of DM halo masses such that the number of halos per unit volume in the mass range M to $M + \delta M$ is given by

$$\frac{dn}{dM}(M,t) = \left(\frac{2}{\pi}\right)^{\frac{1}{2}} \frac{\rho_0}{M^2} \frac{\delta_c(t)}{\sigma(M)} \left|\frac{d\ln\sigma}{d\ln M}\right| \exp\left[-\frac{\delta_c^2(t)}{2\sigma^2(M)}\right], \tag{2.3.1}$$

where ρ_0 is the mean density of the universe, $\sigma(M)$ is the fractional root variance in the density field smoothed using a top-hat filter that contains, on average, a mass M, and $\delta_c(t)$ is the critical overdensity for spherical top-hat collapse at time t (Eke et al., 1996).

Different studies tried to fit the formalism of Press and Schechter (1974) with modern N-body measurements of the halo mass function. Different attempts to calibrate the halo mass function applied different filters and barriers (e.g., Sheth et al., 2001), but it is impossible to reproduce accurately without adjustment

parameters. The best fitting formula is the result of the work of Tinker et al. (2008) where equation 2.3.1 takes the following form

$$\frac{dn}{dM} = f(\sigma)\frac{\bar{\rho}}{M}\frac{d\ln\sigma^{-1}}{dM}, \tag{2.3.2}$$

where

$$f(\sigma) = A\left[\left(\frac{\sigma}{b}\right)^{-a} + 1\right]\exp\left(-\frac{c}{\sigma^2}\right), \tag{2.3.3}$$

with A, a, b and c free parameters determined by fitting the results of N-body simulations, the mass variance $\sigma^2(M)$ is determined from the power spectrum of density fluctuations

$$\sigma^2(M) = \frac{1}{2\pi^2}\int_0^\infty P(k)T^2(k)\hat{W}_M(k)k^2dk, \tag{2.3.4}$$

where $P(k)$ is the primordial power spectrum, $T(k)$ is the cold dark matter transfer function (Eisenstein and Hu, 1999) and $\hat{W}_M(k)$ is the Fourier transform of the real-space top-hat window function. These formalisms are important, as they are the basis of algorithms for building DM merger trees.

Until now, we describe how DM halos form and distribute, but to characterize a DM halo we define an overdensity Δ, which defines the virial radius of the halo. The overdensity of recently collapsed halos with respect to the field is approximately 200 times (in a spherical top-hat collapse model, e.g. Eke et al., 1996), the virial radius is given by

$$r_v = \left(\frac{3M}{4\pi\rho_0\Delta}\right)^{\frac{1}{3}}. \tag{2.3.5}$$

N-body simulations indicate that density profiles of almost all DM halos can be described in a universal form in CDM cosmologies. This profile is the Einasto profile (Einasto, 1965) and is better than the Navarro-Frenk-White (NFW) profile (Navarro et al., 1996, 1997). The profile is given by

$$\rho(r) = \rho_{-2}\exp\left(-\frac{2}{\alpha}\left[\left(\frac{r}{r_{-2}}\right)^{\alpha} - 1\right]\right), \tag{2.3.6}$$

where r_{-2} is a characteristic radius at which the logarithmic slope of the density profile equals -2, ρ_{-2} is a normalization factor, r is the distance from the center

of the halo and α is a parameter which controls how rapidly the logarithmic slope varies with radius (Benson, 2010).

2.4 Evolution of baryons

The initial distribution of baryonic matter is assumed to be approximately uniform, and trace the dark matter distribution on scales above the Jeans length (Arons and Silk, 1968; Gnedin and Hui, 1998). Baryons move to the deepest potential inside DM haloes, and concentrate there.

This process is known as accretion of baryons. The amount of baryons that are accreted from the Intergalactic Medium (IGM) depends on the depth of the DM halo potential and the pressure of the baryons.

The concept of cooling involves a variety of processes, but the main concept is that the initial gas that is subjected to a powerful virial shock will have its kinetic energy converted to thermal energy, raising its temperature to approximately the virial temperature and reaching the hydrostatic equilibrium.

This hot halo gas can cool radiatively and will eventually lose energy. Of course, there are different mechanisms to accelerate the cooling process; atomic cooling, Compton cooling, and molecular hydrogen cooling.

The cooling process is relevant to form dense clouds, where star formation begins. However, there are different processes that suppress (or destroy) the formation of these clouds as a result of heating. For example, photoheating, heating from feedback, preheating and thermal conduction (Benson, 2010).

2.5 Galaxy-Galaxy interactions

We know that galaxies are not all isolated. There is evidence of strong interactions between galaxies in their large-scale environment, and these interactions can affect the evolution of galaxies. Furthermore, there are different types of interactions between galaxies (i.e., galaxy orbits, gravitational interactions and hydrodynamical interactions).

For a long time, numerical simulations indicated that any information from previous generations of halos is lost after a merging process (Katz and White,

1993; Summers et al., 1995).

The article of Tormen et al. (1998); Moore et al. (1999); Klypin et al. (1999) demonstrate that it was a numerical issue and not physical reasonable. In other words, DM halos can survive after merger and persist as subhalos within larger halos.

In high-resolution simulations (e.g., Kuhlen et al., 2008; Springel et al., 2008) there is evidence of multiple levels of subclustering (i.e., subhalos within subhalos).

The largest halo is called host halo, whereas the halo that mergerd is called subhalo. Both are gravitationally bound, and consequently the subhalo is orbiting its host. The orbit of the sub-halo can interact with the galaxy in the host halo. This is called the orbit interaction of galaxies.

When we consider gravity affecting the orbit of such subhalos, there must be a dissipative process to reduce their orbital energies. This means that subhalos reduce their orbital energy to move in orbits close to the center of the host galaxy. One mechanism is dynamical friction (Chandrasekhar, 1943). Dynamical friction tends to drag subhalos down towards the center of their host halo, where they may merge with any other galaxy that finds itself there.

Tidal destruction is another process that can occur. When a subhalo and its galaxy orbit each other, they experience tidal forces that can strip away the outer parts of the galaxy or, in extreme cases, completely break it apart, forming a stellar stream (an example is the Sagittarius dwarf galaxy in orbit around the Milky Way Belokurov et al., 2006).

If the tidal interaction is not enough to remove material from the galaxy, the tidal forces can heat the galaxy. This is the result of the energy transference from the orbit to internal motions of stars in the galaxy. Heating can destroy cold structures such as disks (Moore et al., 1996, 1998; Mayer et al., 2001b,a; Gnedin, 2003; Mastropietro et al., 2005a,b). This happens because stars experience a rapidly changing tidal field along its orbit and gain energy in the form of random motions, leading to the system expanding and becoming dynamically hotter.

Finally, the hydrodynamical interaction refers to the baryonic content of galaxies. The collisionless DM is affected only by gravity, but the baryonic content of

galaxies can be strongly affected by hydrodynamical forces.

An example is the ram pressure, where a subhalo moves through the hot atmosphere of a host halo. The relative motion of the galaxy moving through the intracluster medium causes a drag force to be exerted on the galaxy. In consequence, the gas of the galaxy is stripped.

2.6 Galaxy structure formation

We know of different components of galaxies. Every structure was formed from different processes. Here we describe the formation of the disk and the spheroid component. Of course, there are more structures, but we refer to Kormendy (1982) for a detailed introduction to this topic.

2.6.1 Galactic disk

The formation of a disk is related to the conservation of angular momentum. The process starts with a gas cloud that collapses under gravity. Eventually, the collapse stops when the system is rotationally supporteda and the angular momentum of the gas will form a disk. This process is analogous to that of DM halos, namely tidal torques from the surrounding large-scale structure (Hoyle et al., 1949).

It is possible to find the size of the disk by solving

$$\frac{j^2(M)}{R^3(M)} = \frac{\partial}{\partial R}\Phi(M), \tag{2.6.1}$$

where $j(M)$ is the specific angular momentum enclosing mass M and this equation is solved for $R(M)$. The potential $\Phi(M)$ is the sum of the self-gravity of the disk and that of any external potential. Many authors have explored the physics of the disk. A summary can be found in Mo et al. (1998); Mao et al. (1998).

Of course, disks are not completely thin. Disk galaxies show a vertical extension, and the origin of this structure is still unclear. Until now there have been two theories: internal origins (dynamical heating) and external origins (related to accretion).

2.6.2 Galactic spheroid

The formation of spheroids can proceed in two distinct ways. The first way is the destruction of preexisting stellar systems in major mergers. This is a consequence of hierarchical galaxy formation.

When two galaxies with comparable masses merge we may expect significant changes in their structure and the formation of a merger remnant. This is due to the violent relaxation process (Lynden-Bell, 1967). In this process, after the merge the energy of the orbits undergoes orders of unity changes (due to the rapid change in the potential) and randomizes the orbits (Tremaine et al., 1986). This can turn the ordered motions of disks into the random motions seen in spheroids.

The second way is the result of the evolution of galactic disks. The dynamics of self-gravitating disk systems naturally leads to the formation of spheroids. For example, bars can redistribute mass and angular momentum to the build-up of dense central mass concentrations, reminiscent in many ways of bulges formed through mergers.

The size of the resultant spheroid depends, of course, on the formation mechanism. A simple estimation of the size is computed by Cole et al. (2000), where the final radius of the merger remnant (r_f) is give by

$$\frac{c_f G(M_1+M_2)}{r_f} = \frac{c_1 G M_1^2}{r_1} + \frac{c_2 G M_2^2}{r_2} + \frac{f_{\rm orbit} G M_1 M_2}{r_1+r_2}, \tag{2.6.2}$$

where two merging galaxies have masses M_1 and M_2 and half-mass radii r_1 and r_2 respectively. The c coefficients relate the binding energy to the characteristic value of GM^2/r and depend on the density distribution of the galaxy.

2.7 Star formation and feedback

Star formation process converts gas into stars. The key ingredients which regulate this are turbulence, magnetic fields, and self-gravity leading to interactions to form molecular clouds and stars.

There are different attempts to model the star formation in galaxies.

A simple law is the Schmidt-Kennicutt law (Schmidt, 1959; Kennicutt, 1989,

1998). This law relates the rate of star formation per unit of surface area, $\dot{\Sigma}_\star$, with the surface density of the gas, $\Sigma_{\rm gas}$ as $\dot{\Sigma}_\star \propto \Sigma_{\rm gas}^{1.4}$.

Another model for star formation is given by Krumholz and Tan (2007). In this model stars form in molecular clouds and so it is natural that it would be the density of molecular gas (rather than the total gas).

The problem with almost all star formation models is that they give a star formation rate but there is no physical motivation, and it is not possible to guarantee that the model is accurate outside of the conditions in which it was initially observed.

Another important physical process is feedback. Feedback regulates the cooling of the gas. There exists different types of feedback. In the high-mass star and cluster-forming region W51 there is evidence of thermal feedback. During the process of forming, these high-mass stars heat a large volume and a large mass of gas in their neighborhood (Ginsburg et al., 2017). Supernova explosions are another type of feedback, often called kinetic feedback. The supernova explosion removes gas from the galaxy, affecting the amount of gas available for star formation (Lucas et al., 2020). Additionally, the building of BHs in galaxies produces feedback and affects the evolution of the galaxy (Benson et al., 2003). The accretion of material from the accretion disk of the BH triggers a response of radiation and/or mechanical outflow. It is known that if there is radiative feedback, there is also mechanical feedback. If there is only radiative feedback, the predicted BHs mass is larger than the observed (Ciotti et al., 2009). However, mechanical feedback alone can regulate the growth of the BHs and the Active Galactic Nucleus (AGN) activity can effectively expel gas from a galaxy. (Springel et al., 2005a; Di Matteo et al., 2005; Sijacki et al., 2007, 2010; Booth and Schaye, 2009).

2.8 Chemical enrichment

As mentioned in Section 1.1.2. The first generation of stars (Pop. III) must have formed from primordial gas which is metal free. Stellar nucleosynthesis and stellar winds and supernova explosions with heavy elements have a significant impact on the chemical enrichment of the Universe. The presence of different heavy elements significantly alters the rate at which the gas can cool and allows the formation of dust.

This enrichment strongly depends on the stellar population model. It is possible to estimate the fraction of material returned to the Interstellar Medium (ISM). Taking the initial mass function of Chabrier (2003) leads to around 40% of the mass being recycled after 10 Gyr and to around 30% at 1 Gyr.

In the context of numerical galaxy formation models, the process of chemical enrichment is simplified by adopting the instantaneous recycling approximation. In this approximation, mass and metals are assumed to return instantaneously to the ISM after the formation of a population of stars.

2.9 Computational techniques

There are different techniques for galaxy modeling. The two major approaches that have been developed are numerical N-body simulations, which attempt to directly and numerically solve the fully nonlinear equations governing the physical processes. The second, semi-analytic modeling, attempts to construct a coherent set of analytic approximations which describe the same physics.

In recent years a different, a third more empirical approach, utilizing so-called "halo occupation distributions" has become widely used.

All techniques have strengths and weaknesses, and choosing one or another depends on the science you want to do. Here, we introduce the aim of each technique.

2.9.1 Numerical N-body/Hidrodynamical

The most accurate computational method. This solves the physics of galaxy formation via direct simulation, in which the fundamental equations of gravitation, hydrodynamics, and perhaps radiative cooling and transfer are solved for a large number of points.

In this scheme, it is common to model dark matter as collisionless, since it responds only to the gravitational force. For the velocities and gravitational fields occurring during structure and galaxy formation non-relativistic Newtonian dynamics is enough for solving the evolution of the initial distribution of dark matter. This initial distribution is usually a Gaussian random field of density perturbations consistent with the power spectrum of the CMB.

A problem related to this method is the contribution of all particles that act on a single particle. In practice, numerical techniques, such as particle mesh (Kravtsov et al., 1997) and tree algorithms (Springel, 2005), are used to reduce this problem into something more computationally inexpensive.

To study galaxy formation, dark matter alone is insufficient, and baryonic material must be added. This makes the problem much more difficult since at least the pressure forces must be computed and the internal energy of the baryonic matter must be tracked. To add the baryonic component, particle-based methods (e.g., Smoothed Particle Hydrodynamics (SPH), Springel, 2005) have been successful. SPH is a computational method that is used in astrophysics to simulate solid mechanics and fluid flows. Another technique developed for this purpose is the Eulerian grid method (Ricker et al., 2000; Fryxell et al., 2000; Plewa and Müller, 2001; Quilis, 2004). In Eulerian methods, there is a fixed space subdivided by a regular grid where the parameters of the fluid (density, velocity, etc.) are calculated per cell.

On large scales, these methods work well. The problem arises when we explore the process below the resolution of the simulation. The treatment of physics is often at the "subgrid" level and the semi-analytic approach is used.

2.9.2 Semi-Analytic

The semi-analytic technique treats the various physical processes associated with galaxy formation using approximate analytic techniques in order to reduce computational resources. The degree of approximation varies considerably with the complexity of the physics being treated.

Semi-analytical models are calibrated to match N-body/hydrodynamic simulations. This allows the construction of samples of galaxies orders of magnitude larger than possible with N-body techniques. This is useful for a rapid exploration of the parameter space and the model space (Henriques et al., 2009). The primary disadvantage is that they involve a higher degree of approximation.

Some examples of semi-analytical models are GALFORM (Cole et al., 2000), SAGE (Croton et al., 2016) and Galacticus (Benson, 2012). All of them have differences in the implemented prescription of physics. However, all of them are able to reproduce and give insights into the galaxy observables.

2.9.3 Halo occupation distribution

Many authors have demonstrated that the Halo Occupation Distribution (HOD) can fit a wide variety of galaxy data. The HOD scheme is used to study galaxy clustering (e.g. Benson et al., 2000) and they map observable properties of galaxies onto properties of dark matter halos, but do not include actual modeling of physical processes.

In the HOD framework, the relation between the galaxy and matter distributions is fully defined by the probability distribution that a halo of virial mass M contains N galaxies ($P(N|M)$), the relation between the galaxy and the spatial distributions of DM within halos, and the relation between the galaxy and the velocity distributions of dark matter within the halo (Berlind and Weinberg, 2002).

This empirical model, as simple as it is, predicts the galaxy-halo connection quite well, and is useful to describe the galaxy formation history and to generate mock catalogs.

Chapter 3

GALACTICUS

GALACTICUS is a semi-analytic code of galaxy formation and evolution developed by Benson (2012). As a semi-analytic model, it works solving equations describing the evolution of galaxies in a merging hierarchy of DM halos in a DM-dominated universe. Although GALACTICUS can solve galaxies in this context, it also provides other functionalities, such as computing halo mass functions, power spectra, analyzing particle simulations, and performing Markov-Chain-Monte-Carlo (MCMC) simulations.

GALACTICUS is designed to be modular and easily extensible to all its functionality. This feature makes GALACTICUS a powerful tool, due to our understanding of galaxy formation being a fast evolving field.

The main characteristics of GALACTICUS are summarized in three features: extensible implementations for all functions, modular components for tree nodes, and a centralized Ordinary Differential Equations (ODE) solver.

Tree nodes are DM merger trees plus node components. A dark matter merger tree is the merging history of DM halos from small clumps to larger objects (see Fig. 3.0.1).

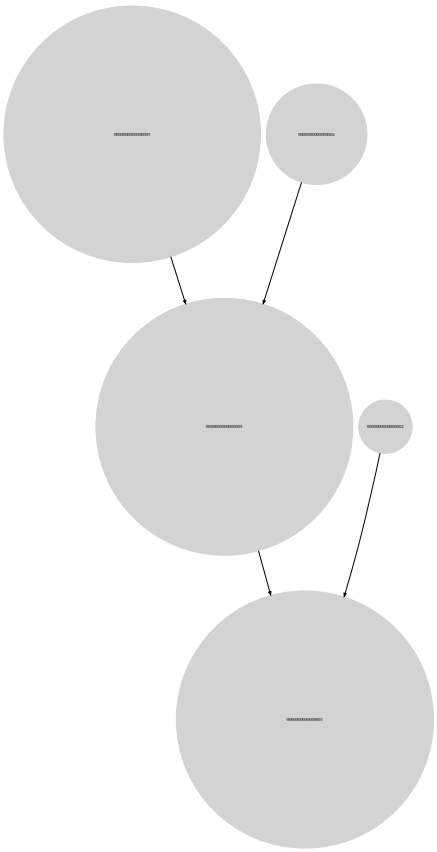

Figure 3.0.1: Visual representation of a single merger tree history constructed with Galacticus. The final DM halo is at $z = 0$. All the halos are scaled with the logarithm of the mass. The figure is automatically constructed within Galacticus.

Source: Galacticus output

A node represents a single DM halo (or sub-halo) along with everything inside it, such as gas, stars, BHs, etc. Each thing a node may contain is called a "component".

The evolution of the equations which describe how the components are interacting in a node is managed by the central ODE solver.

3.1 Coding Galacticus

The process of writing code in Galacticus depends on what exactly you want to do. Usually, minor modifications include writing new classes and functions

which components can require for their evolution depending on the assumed physics. This modifications are usually written in Fortran and XML. Major modifications could include C.

In this work, we implement a new component in Galacticus. This involves more work, but the fundamentals are the same; write new classes and functions and define how the new component is related to the other.

3.1.1 Component definition

Each node in the merger tree consists of an arbitrary number of components. Each component represents a specific class of object, which could be a DM halo, a BH, a galactic spheroid, etc.

A component of each class may consist of one or more different implementations of that component class; these implementations represent the properties of the component (stellar mass, gas mass, size, etc.). For example, the disk component class has three different classes; simple, simple-sized, and standard. The difference between these classes is the properties defined and the differential equations which describe the physical processes. Some functions (or classes) require a specific class due to the dependence on properties, which might not exist in one class but it does in other.

Additionally, each component contains methods (functions) which can be used to access its properties, query its interfaces, and which are used internally to perform ODE evolution, output, etc.

3.1.2 Implementing a new component

Implementing a new component involves writing modules, classes, and functions (and the interface to tell Galacticus how to link the new component). The code needs to handle initialization, creation, evolution, and responses to any events. Everything that can interrupt suddenly the evolution of the properties (for example mergers of galaxies).

There is a convention to define a new component. The code is split into three or four files, although some components might not need all of these files. In this thesis, we split the component definition into three files:

`objects.nodes.components.NuclearStarCluster.F90` The primary file that describes the NSC component and its properties. This file also contains functions to manipulate the component evolution through a merger tree. In other words, the scales for the ODE solver, the behavior during mergers, etc.

`objects.nodes.components.NuclearStarCluster.bound_functions.F90` Contains functions that will be bound to the component object. These functions will include any functions that get or set values of properties in the component. In our case, it is relevant to define functions to calculate the radius and the velocity of the cluster.

`objects.nodes.components.NuclearStarCluster.data.F90` Contains any data that may need to be shared between the above two files. These contain parameters which control some property of the component that is the same for all instances (e.g. the values to normalize the equation describing the radii evolution in NSCs).

In the `objects.nodes.components.NuclearStarCluster.F90`, the component definition itself takes the form of an embedded XML document. A minimal example is as follows:

```
<component>
<class>NSC</class>
<name>standard</name>
<isDefault>true</isDefault>
<properties>
 <property>
  <name>isInitialized</name>
  <type>logical</type>
  <rank>0</rank>
  <attributes isSettable="true" isGettable="true" isEvolvable="false" />
 </property>
    ...
    ...
</properties>
<functions>
```

```
objects.nodes.components.NuclearStarCluster.standard.bound_functions.inc
</functions>
</component>
```

The definition begins with the tag `<component>` which indicates that we are defining a new component. The tag requires additional information:

`class` The name of the class is the name of the type of the component, in our case the name is NSC.

`name` The name of the component refers to the implementation of the class. Here we define the name of the [`class`] as [`standard`].

`isDefault` Specifies whether this should be the default implementation of this class. It is important if we define more than one implementation.

`properties` Contains an array with the property elements of this implementation. Each defined property should have extra information about its implementation:

- `name` The name of the property.
- `type` The type can be `real, logic, abundances, chemical or KeplerOrbit`.
- `rank` It is 0 if the property is a scalar or 1 for an 1-D array.
- `attributes` The attributes are characteristics of the property, this control if the property can be called for other modules.
  - `isSettable` If true then the value of this property can be set directory.
  - `isGettable` If true, then the value of this property can be obtained from the directory.
  - `isEvolvable` If true, this property evolves as part of the Galacticus ODE system.
- `function` The name of the file which contains the bound functions of the component.

Depending on the property, more/less information can be required to link the

property with other modules/functions in Galacticus.

3.1.2.1 Component Initialization

When a component is defined, it is important to create a module for its initialization. This is to avoid duplication of components in the nodes when performing calculations. Without this module, Galacticus can solve two (or more) copies of the component in one galaxy.

It is important to note that initialization is not the same as creation. Initializing a component is the previous step before creation, and it is useful to read the parameters or allocate the workspace before creation and the evolution of the component. In general, components are created in response to events. In our case, NSCs are created in response to star formation in the spheroidal component of the host galaxy.

3.1.2.2 Component Evolution

We mentioned that the defined component has properties that are described by attributes. Each property with an isEvolvable attribute set to true is included in the ODE solver of Galacticus. Otherwise, the property can be computed analytically with an internal function.

That means Galacticus will create two functions that allow the rate of change of a property to be adjusted and the absolute scale used in the ODE error control to be set. The first one is a rate compute function. This should be defined to perform any calculations necessary to determine the rate of change of the property and adjust the rate appropriately.

3.1.2.3 Evolution Interrupts

It is often necessary to interrupt the smooth ODE evolution of a node in Galacticus.

For example, if a galaxy merges with another galaxy (in this case, the evolution of the properties must be stopped and handle the merger) or if a component must be created before evolution can continue (e.g. there is a spheroidal galaxy and at some point of the evolution a disk needs to be created).

The rate adjust and rate compute subroutines allow for interrupts to be flagged via their interrupt and interrupt procedure arguments. If an interrupt is required, then interrupt should be set to true, while interruptProcedure should be set to point to a procedure which will handle the interrupt. Then, provided no other interrupt occurred earlier, the evolution will be stopped and the interrupt procedure called before evolution is continued.

Chapter 4

Model implementation in GALACTICUS

In this chapter, we describe the physics of the NSC model and the BH formation scenario implemented in the GALACTICUS code.

4.1 Nuclear star cluster model

As we mentioned in Section1.2.1, there are different mechanisms to explain the presence of NSCs in the center of galaxies. For this work, we assume that NSCs are formed from the cold gas accumulated in the center of the galaxy. The gas transfer rate to the center is assumed to be correlated with the global star formation rate in the galaxy, leading to the formation of NSCs through in situ star formation at the galactic center, as in the model of Barausse (2012) and its improvement made by Sesana et al. (2014). The rate is given by the relation used by Graham and Spitler (2009); Haiman et al. (2004); Lapi et al. (2014); Antonini et al. (2015),

$$\dot{M}_{\rm gas}^{\rm NSC} = A_{\rm res}\psi_{\rm bulge}, \tag{4.1.1}$$

where $\psi_{\rm bulge}$ is the star formation in the bulge, and $A_{\rm res} \approx 10^{-3} - 10^{-2}$ is a free parameter (Sesana et al., 2014; Antonini et al., 2015).

Furthermore, we need to provide to GALACTICUS a mass distribution for the NSC, due to the dependence with other functions (i.e. the computation of the half-mass radius, surface density). This is not an easy choice; it is hard to directly

observe the structure (or resolve the kinematics) of NSCs and find the mass distribution of these objects. An important tool is integral field spectroscopy, which reveals substructures within the NSCs (Neumayer et al., 2020), providing some information about the real distribution. In the same work, many NSCs appear to be nonspherical, and the observations of edge-on spirals by Seth et al. (2006) identified elongated disk-like structures in NSCs.

The mass distribution for NSCs is a Sérsic profile with $n = 2.28$ (Pechetti et al., 2020).

The size of the NSC is not easy to define. There is no agreement between the models describing the distribution of stars in NSCs. However, it is assumed that the radius scales with the square root of the luminosity (Turner et al., 2012; Antonini et al., 2015; Neumayer et al., 2020).

$$r_{\rm NSC} = r_0\ [\rm pc] \cdot \sqrt{\frac{M_{\rm dyn}}{10^6\, M_\odot}}. \tag{4.1.2}$$

In equation 4.1.2, the dynamical mass is defined as $M_{\rm dyn} = M_{\rm gas}^{\rm NSC} + M_\star^{\rm NSC}$. Furthermore, we fix the value of $r_0 = 3.3$ [pc] as this is the mean size of the observed NSCs (Neumayer et al., 2020). We also include an efficiency parameter $\epsilon_{\rm r}$ used to calculate the critical mass of NSCs. The parameter rescales the radius $r_{\rm NSC} \rightarrow \epsilon_{\rm r} r_{\rm NSC}$ with $0 < \epsilon_{\rm r} \leq 1$ an input parameter.

We compute the velocity of NSC at a given radius, as the orbital velocity of the dynamical mass,

$$v_{\rm NSC}(r) = \sqrt{\frac{G M_{\rm dyn}^{\rm NSC}}{r_{\rm NSC}}}. \tag{4.1.3}$$

The star formation rate in NSCs is assumed to occur in a 'quiescent' star formation mode for our nuclear gas reservoir as in Sesana et al. (2014),

$$\dot{M}_\star^{\rm NSC} = f_c \frac{M_{\rm gas}^{\rm NSC}}{t_{\rm SF}}. \tag{4.1.4}$$

The interpretation of equation 4.1.4 is that star formation in the gas reservoir takes place on a timescale $t_{\rm SF}$, previously modeled by Krumholz et al. (2009) and improved by Sesana et al. (2014). Star formation is assumed to occur in clouds

and involves only a fraction f_c of the cold gas available in the reservoir.

$$t_{\rm SF}^{-1} = (2.6\ {\rm Gyr})^{-1} \times \begin{cases} \left(\frac{\Sigma_{\rm res}}{\Sigma_{\rm th}}\right)^{-0.33} & , \Sigma_{\rm res} < \Sigma_{\rm th}, \\ \left(\frac{\Sigma_{\rm res}}{\Sigma_{\rm th}}\right)^{0.34} & , \Sigma_{\rm res} > \Sigma_{\rm th} \end{cases}, \tag{4.1.5}$$

with $\Sigma_{\rm th} = 85\ M_\odot\,{\rm pc}^{-2}$ and $\Sigma_{\rm res} = \frac{M_{\rm gas}^{\rm NSC}}{4\pi r_{\rm NSC}^2}$ the surface density of the reservoir for an spherical mass distribution. The meaning of two branches in Equation 4.1.5 is that the cloud density is determined by internal processes or by the external pressure in galaxies with large surface densities.

Furthermore, the fraction of cold gas available for star formation strongly depends on the fraction of molecular gas. For metallicities $Z > 0.01$ (relative to the solar metallicity), star formation occurs in molecular clouds. On the other hand, if $Z < 0.01$, the star formation takes place in the atomic phase of the gas (Krumholz, 2012). This is summarized in Equation 4.1.6:

$$f_c = \begin{cases} 1 - \left[1 + \left(\frac{3}{4}\frac{s}{1+\delta}\right)^{-5}\right]^{-\frac{1}{5}} & , \text{if } f_c > 2\%, \\ 2\% & , \text{otherwise} \end{cases} \tag{4.1.6}$$

where

$$s = \frac{\ln(1+0.6\chi)}{0.04\Sigma_1 Z}, \tag{4.1.7}$$

$$\chi = 0.77(1+3.1Z^{0.365}), \tag{4.1.8}$$

$$\delta = 0.0712(0.1s^{-1}+0.675)^{-2.8}, \tag{4.1.9}$$

$$\Sigma_1 = \frac{\Sigma_{\rm res}}{M_\odot\,{\rm pc}^{-2}}. \tag{4.1.10}$$

Finally, we need to estimate the stellar age of the system. Stellar age depends on the ratio of old and young stars that determines the 'age' observed. In order to do that, we use equation 4.1.11. This expression corresponds to the mass-weighted age:

$$\langle t \rangle = t - \int_0^t dt' t' \dot{M}(t') \int_0^t dt' \dot{M}(t'), \tag{4.1.11}$$

where $\dot{M}(t')$ is the star formation rate at time t', and t is the present time of the NSC.

4.2 Nuclear star cluster collapse

In this Section, we describe the model for the formation of BH seeds inside NSCs. This scenario is completely based on the work of Escala (2021). His work shows that it is possible to form BHs in NSCs in virial equilibrium, with masses larger than 10^8 $M_\odot$ and with short collision times. For extremely dense stellar systems, it means they will be globally stable against collisions, leading to a destabilization of the cluster and collapse into a central massive object.

To quantify the role of collisions in NSCs, it is important to define the collision timescale $t_{\rm coll}$. This timescale quantifies how frequent collisions are in any system with a large number of particles (in this case, stars).

The collision timescale depends on the characteristic (dispersion) velocity σ of the system and the particle (star) mean free path λ (Binney and Tremaine, 2008), leading to $t_{\rm coll} = \frac{\lambda}{\sigma}$. The value of σ in a virialized system is $\sigma \approx \sqrt{\frac{GM}{R}}$, with M and R the stellar mass and the radius of the NSC. It is possible to determine the probabilistic mean free path for a system with a number density of stars n and the effective cross section Σ_0 as $\lambda n \Sigma_0 = 1$ (Landau and Lifshitz, 2013; Shu, 1991). Using these expressions it may be easy to show that the collision timescale is equivalent to

$$t_{\rm coll} = \frac{\lambda}{\sigma} = \frac{\frac{1}{n\Sigma_0}}{\sqrt{\frac{GM}{R}}}, \tag{4.2.1}$$

$$t_{\rm coll} = \sqrt{\frac{R}{GM(n\Sigma_0)^2}}. \tag{4.2.2}$$

The numerical density n of stars with mass $M_\star$ and radius $R_\star$ in a cluster with a total stellar mass M, radius R, and a total number of stars $N = M/M_\star$, is obtained dividing the total number of stars and the volume of the cluster.

$$n = \frac{N}{V} = \frac{3}{4\pi}\frac{M}{M_\star}\frac{1}{R^3}. \tag{4.2.3}$$

Replacing the number density in the Equation 4.2.2 we obtain:

$$\begin{aligned} t_{\rm coll} &= \left[\frac{R}{GM\left(\frac{3}{4\pi}\frac{M}{M_\star}\frac{1}{R^3}\Sigma_0\right)^2}\right]^{\frac{1}{2}}, \\ M^3 &= R^7\left(\frac{4\pi}{3}\frac{1}{t_{\rm coll}}\frac{M_\star}{\Sigma_0 G^{\frac{1}{2}}}\right)^2, \\ M &= R^{\frac{7}{3}}\left(\frac{4\pi}{3}\frac{1}{t_{\rm coll}}\frac{M_\star}{\Sigma_0 G^{\frac{1}{2}}}\right)^{\frac{2}{3}}. \end{aligned} \tag{4.2.4}$$

From equation 4.2.4, if the age of the system $t_{\rm H}$ is comparable to the collision time of the system ($t_{\rm coll} \leq t_{\rm H}$), we can define the critical mass

$$M_{\rm crit}(R) = R^{\frac{7}{3}}\left(\frac{4\pi}{3}\frac{M_\star}{t_{\rm H}\Sigma_0 G^{\frac{1}{2}}}\right)^{\frac{2}{3}}, \tag{4.2.5}$$

where $\Sigma_0 = 16\sqrt{\pi}(1+\Theta)R_\star^2$, with $\Theta = 9.54((M_\star R_\odot)/(M_\odot R_\star))(100\ {\rm km\,s^{-1}}/\sigma)^2$. The defined critical mass gives the condition for the formation of a BH seed in Galacticus.

We also introduce a mass threshold parameter to avoid the collapse of NSCs in masses below the specified value.

4.3 Black hole formation

Originally, Galacticus assumes that every galaxy hosts a SMBH seed in its center. The initial mass ($M_\bullet$) of the seed is set as an input parameter.

Now, we introduce a new mechanism into the code to form BH seeds. If the stellar mass of NSC is greater than the critical mass $M_\star^{\rm NSC} > M_{\rm crit}$ and a mass threshold ($M_{\rm Threshold}$), a new seed is formed in the center of the galaxy and then merges instantly with the previous seed in the center of the host galaxy. The new BH seed has a mass proportional to the stellar mass of the system attenuated by a free efficiency parameter ϵ (see equation 4.3.1).

$$M_\bullet = \epsilon_\bullet M_\star^{\rm NSC}, \tag{4.3.1}$$

4.4 Black hole growth

The evolution of the black hole mass is given by

$$\dot{M}_\bullet = (1 - \epsilon_{\rm radiation} - \epsilon_{\rm jet})\dot{M}_0, \tag{4.4.1}$$

where $\epsilon_{\rm radiation}$ is the radiative efficiency of the accretion flow feeding the black hole, $\epsilon_{\rm jet}$ is the efficiency with which accretion power is converted to jet power, and $\dot{M}_0$ is the rest mass accretion rate. This rate is computed assuming Bondi-Hoyle-Lyttleton accretion from the spheroid gas reservoir (with an assumed temperature of $T_{\rm spheroid}$) enhanced by a factor of α, and from the Circumgalactic Medium (CGM). The gas clouds are assumed to be not self-gravitating and uniform at infinity.

The explicit equation for $\dot{M}_0$ is

$$\dot{M}_0 = \dot{M}_{\bullet,\rm spheroid} + \dot{M}_{\bullet,\rm CGM}, \tag{4.4.2}$$

where

$$\dot{M}_{\bullet,\rm spheroid} = \frac{4\pi G^2 M_\bullet^2 \rho_{\rm gas,spheroid}}{c_s^3}, \tag{4.4.3}$$

with c_s the sound speed in the gas (assumed to be ideal and with temperature $T_{\rm spheroid}$) (Edgar, 2004). The contribution of CGM is calculated the same as for the spheroid component, resulting in

$$\dot{M}_{\bullet,\rm CGM} = \frac{4\pi G^2 M_\bullet^2 \rho_{\rm gas,CGM}}{c_s^3}, \tag{4.4.4}$$

with and c_s the sound speed in the CGM gas with the temperature of the CGM assuming a virial profile.

The second mechanism to increase the mass of BHs is due to mergers; in these mergers, it is assumed that the resulting properties follow the model of Rezzolla et al. (2008). This computes the resulting spin from a binary merger and assumes that there is negligible energy loss after the emission of gravitational waves, resulting in a new BH with mass $M_{\bullet,\rm new}$ given by

$$M_{\bullet,\rm new} = M_{\bullet,1} + M_{\bullet,2}, \tag{4.4.5}$$

where $M_{\bullet,1}$ is the most massive BH and $M_{\bullet,2}$ is the less massive BH.

4.4.1 Contribution from the nuclear star cluster to the BH accretion rate

Our reservoir of gas for the NSC contributes to the accretion rate, introducing a new term in the equation 4.4.2:

$$\dot{M}_0 = \dot{M}_{\bullet,\mathrm{spheroid}} + \dot{M}_{\bullet.\mathrm{CGM}} + \dot{M}_{\bullet,\mathrm{NSC}}, \tag{4.4.6}$$

where $\dot{M}_{\bullet,\mathrm{NSC}}$ is analogous to the accretion contribution from the spheroid component (see the first term on the right side in equation 4.4.3):

$$\dot{M}_{\bullet,\mathrm{NSC}} = \frac{4\pi G^2 M_\bullet^2 \rho_{\mathrm{gas,NSC}}}{c_s^3}, \tag{4.4.7}$$

with c_s the sound speed for an ideal gas with an assumed temperature $T = 100\,\mathrm{K}$, which is the same temperature of the bulge.

Chapter 5

Simulations

In this chapter, we talk about the set up of simulations run in Galacticus. We briefly describe the receipts for our simulations and, of course, the theory behind them. We start from the best baryonic model constrained in Galacticus.

We use the evolveForests task provided by Galacticus. This task generates a set of merger trees for DM halos and then evolves them forward in time according to whatever physics specified in the parameter file.

5.1 Cosmology and structures growth

First, we need to fix the cosmological model. We start by selecting 'matterLambda' functions. This means that all the cosmological functions in function of time are computed assuming a universe containing collisionless matter and a cosmological constant Λ.

The cosmological parameters of our model are $H_0 = 67.36$, $\Omega_M = 0.3153$, $\Omega_\Lambda = 0.6847$, $\Omega_b = 0.0493$ and $T_{\rm CMB} = 2.72548$ (Planck Collaboration et al., 2020).

Once the cosmological background is fixed, we specify the linear theory power spectrum.

We compute the mass variance of cosmological density fields computed from a filtered power spectrum

$$\sigma^2(M) = \frac{1}{2\pi^2}\int_0^\infty P(k)T^2(k)W^2(k)k^2dk, \tag{5.1.1}$$

where $P(k)$ is the primordial power spectrum, $T(k)$ is the transfer function, and $W(k)$ is the power spectrum variance window function (in this case, just a top-hat function). The mass variance is normalized via the parameter $\sigma_8 = 0.8111$(Planck Collaboration et al., 2020).

The primordial power spectrum is modeled as a power law:

$$P(k) \propto k^{n_s}, \tag{5.1.2}$$

where $n_s = 0.9649$ is the power spectrum index at wavenumber $k_{\text{ref}} = 1.0$ (Planck Collaboration et al., 2020). The transfer function is the fitting formula of Eisenstein and Hu (1999) for the Cold Dark Matter.

The linear growth of cosmological structures is assumed to be collisionless matter, the pressure terms for the growth of baryons are ignored, and there is no wavenumber dependence.

The critical overdensity for the collapse is based on the spherical collapse in a matter plus cosmological constant universe and the same option is chosen for the virial density contrast. For more details, see Percival (2005).

The selected DM halo mass function is Sheth et al. (2001). The form of this mass function is

$$\nu f(\nu) = 2A \left(1 + \frac{1}{\nu'^{2q}}\right) \left(\frac{\nu'^2}{2\pi}\right)^{\frac{1}{2}} \exp\left(-\frac{\nu'^2}{2}\right), \tag{5.1.3}$$

where $\nu' = \sqrt{a}\nu$, $a = 0.707$, $q = 0.3$ and $A = 0.322$.

5.1.1 Dark matter halos

We specify a single level hierarchy to handle the hierarchy of substructures that form as halos merge. This means that a DM halo can contain a subhalo, but the subhalo cannot contain a subhalo.

The density profile selected for the DM halos is the Navarro-Frenk-White profile (Navarro et al., 1996, 1997), and the DM profile concentration uses the fit of Gao

et al. (2008),

$$\log_{10} c = A \log_{10} M_{\rm halo} + B \tag{5.1.4}$$

$$A = -0.140 \exp\left[-\left(\frac{\log_{10} a + 0.05}{0.35}\right)^2\right] \tag{5.1.5}$$

$$B = +2.646 \exp\left[-\left(\frac{\log_{10} a}{0.50}\right)^2\right], \tag{5.1.6}$$

where a is the expansion factor.

The spin of the DM halos is taken from the distribution formula of Bett et al. (2007)

$$P(\log_{10}(\lambda)) = A \left(\frac{\lambda}{\lambda_0}\right)^3 \exp\left[-\alpha \left(\frac{\lambda}{\lambda_0}\right)^{\frac{3}{\alpha}}\right], \tag{5.1.7}$$

where $A = 3 \ln\left(10 \frac{\alpha^{\alpha-1}}{\Gamma(\alpha)}\right)$, $\lambda_0 = 0.04326$, $\alpha = 2.509$ and λ is the dimensionless spin parameter introduced by Peebles (1969).

The DM halo is related to the galactic structure solver. In our case, the sizes of galactic components by assuming that their self-gravity is negligible and baryons do not modify the DM density profile. The radius of a given component is then found by solving

$$j = \sqrt{G M_{DM}(r) r}, \tag{5.1.8}$$

where j is the specific angular momentum of the component, r is radius and $M(r)$ is the mass of DM within radius r.

5.1.2 Circumgalactic physics

The accretion of material from the Intergalactic Medium (IGM) onto the Circumgalactic Medium (CGM) is given by

$$\dot{M}_{\rm accretion} = \begin{cases} \frac{\Omega_{\rm b}}{\Omega_{\rm M}} \dot{M}_{\rm halo} & \text{if } V_{\rm virial} > V_{\rm reionization} \text{ or } z > z_{\rm reionization} \\ 0 & \text{otherwise} \end{cases}, \tag{5.1.9}$$

where $z_{\rm reionization} = 9.97$ (Hinshaw et al., 2013) is the redshift at which the Universe is reionized, $V_{\rm reionization} = 35$ km s^{-1} is the virial velocity below which accretion is suppressed after reionization.

The mass distribution of the CGM is

$$\rho_{\mathrm{CGM}}(r) \propto [r^2 + r_{\mathrm{core}}^2]^{3\beta/2}, \tag{5.1.10}$$

where r_{core} is 0.259 times the virial radius and $\beta = \frac{2}{3}$.

This gas is cooled and feeds the galaxy. The cooling function is computed internally using the Cloudy code.

The cooling radius is computed by finding the radius at which the time available (see equation 5.1.11) for cooling equals the cooling time (see equation 5.1.12).

The available time for cooling is computed using the model of White and Frenk (1991),

$$t_{\mathrm{available}} = \exp\left[f \ln t_{\mathrm{Universe}} + (1-f) \ln t_{\mathrm{dynamical}}\right], \tag{5.1.11}$$

where $f = 0.835$, t_{Universe} is the age of the Universe and $t_{\mathrm{dynamical}}$ is the dynamical time of the CGM.

On the other hand, the cooling time is

$$t_{\mathrm{cool}} = \frac{N}{2} \frac{k_B T n_{\mathrm{tot}}}{\Lambda}, \tag{5.1.12}$$

where $N = 3.0$ is the number of degrees of freedom in the cooling gas with temperature T and Λ is the cooling function (computed by Cloudy).

Finally, the cooling rate is computed using the model of White and Frenk (1991),

$$\dot{M}_{\mathrm{cool}} = 0.659 \cdot \begin{cases} 4\pi r_{\mathrm{infall}}^2 \rho(r_{\mathrm{infall}}) \dot{r_{\mathrm{infall}}} & \text{if } r_{\mathrm{infall}} < r_{\mathrm{CGM,outer}} \\ M_{\mathrm{CGM}} / \tau_{\mathrm{CGM,dynamical}} & \text{if } r_{\mathrm{infall}} \geq r_{\mathrm{CGM,outer}} \end{cases}, \tag{5.1.13}$$

where r_{infall} is the cooling radius, $\rho(r)$ is the CGM mass distribution (see equation 5.1.10), $\tau_{\mathrm{CGM,dynamical}}$ is the dynamical time of the CGM, and $r_{\mathrm{CGM,outer}}$ is the outer radius of the CGM.

5.1.3 Star formation

Star formation in galaxies is separated into two components. The disk and the spheroid components have their own star formation rate.

For the disk component, the star formation rate is given by

$$\dot{M}_{\star}^{\text{disk}} = \frac{M_{\text{gas,disk}}}{\tau_{\text{dynamical,disk}}}, \tag{5.1.14}$$

where $\tau_{\text{dynamical,disk}}$ is the dynamical time of the disk:

$$\tau_{\text{dynamical,disk}} = \epsilon_{\star}^{-1} \tau_{\text{dynamical}} \left(\frac{V}{200 \text{ km s}^{-1}} \right)^{\alpha}, \tag{5.1.15}$$

with $\epsilon_{\star} = 0.2536$, $\alpha = -3.2781$, $\tau_{\text{dynamical}} = r_{\text{disk}}/V_{\text{disk}}$ and this value is not allowed to fall below 1.871 Gyr.

In the same way, the spheroid component uses the same star formation rate receipt:

$$\tau_{\text{dynamical,spheroid}} = \epsilon_{\star}^{-1} \tau_{\text{dynamical}} \left(\frac{V}{200 \text{ km s}^{-1}} \right)^{\alpha}, \tag{5.1.16}$$

with $\epsilon_{\star} = 0.0030$, $\alpha = 1.993$, $\tau_{\text{dynamical}} = r_{\text{spheroid}}/V_{\text{spheroid}}$ for $\tau_{\text{dynamical,spheroid}}$, and this value cannot fall below 13.16 Gyr.

The initial mass function of the stellar population selected is the model of Chabrier (2001), where

$$\phi(M) \propto \begin{cases} M^{-1} \exp\left(-\frac{\left[\frac{\log_{10} \frac{M}{M_c}}{\sigma_c} \right]^2}{2} \right) & \text{for } 0.1 < M \ [M_{\odot}] < 1 \\ M^{0.69} & \text{for } 1 < M \ [M_{\odot}] < 125 \\ 0 & \text{otherwise} \end{cases}, \tag{5.1.17}$$

where $\sigma_c = 0.69$ is the width of the lognormal part of the initial mass function.

The feedback from star formation is modeled as a power law, where the outflow is given by

$$\dot{M}_{\text{outflow}} = \left(\frac{V_{\text{outflow}}}{V} \right)^{\alpha} \frac{\dot{E}}{E_{\text{canonical}}}, \tag{5.1.18}$$

where V_{outflow} is velocity scale at which the supernovae (SNe)- driven outflow rate equals the star formation rate. For the disk component $V_{\text{outflow}} = 49.95 \text{km s}^{-1}$, while for the spheroid component $V_{\text{outflow}} = 41.529 \text{km s}^{-1}$. The exponent is $\alpha = 3.38$ for the disk and $\alpha = 2.47$ for the spheroid component. Furthermore, the outflow is limited to a minimal timescale in units of the dynamical time of each

component. For the disk, it is 0.0004 times the dynamical timescale, while for the spheroid it is 0.002.

5.2 Galaxy mergers

When a satellite merges with its host galaxy, the mass movement is determined by the masses of the satellite ($M_{\rm satellite}$) and the central galaxy ($M_{\rm central}$).

if $M_{\rm satellite} > f_{\rm major} M_{\rm central}$, all mass from both satellite and central galaxies moves to the spheroid component of the central galaxy, with $f_{\rm major} = 0.197$.

Otherwise: Gas from the satellite moves to the dominant component of the central and stars from the satellite moves to the spheroid of the central. The mass in the central galaxy does not move.

The size of the remnant spheroid is computed using the algorithm of Cole et al. (2000):

$$\frac{(M_1 + M_2)^2}{r_{\rm new}} = \frac{M_1^2}{r_1^2} + \frac{M_2^2}{r_2^2} + \frac{f_{\rm orbit}}{c} \frac{M_1 M_2}{r_1 + r_2}, \tag{5.2.1}$$

where M_1 and M_2 are the baryonic masses of the components of the merging galaxies that will end up in the spheroid component of the remnants and r_1 and r_2 are the half mass radii of those same components. $r_{\rm new}$ is the half mass radius of the spheroidal component of the remnant galaxy and $c = 0.5$ is a constant which depends on the distribution of mass and $f_{\rm orbit} = 1.1695$ depends on the orbital parameters of the galaxy pair.

The timescale of the merger is computed using the modifier of Villalobos et al. (2013), where

$$\tau_{\rm merge} = (1 + z)^{\alpha} \tau'_{\rm merge}, \tag{5.2.2}$$

where $\alpha = 0.471$ and $\tau'_{\rm merge}$ is the timescale computed using the dynamical calibration of Jiang et al. (2008). The multiplier value required in their fitting formula is 0.313.

5.2.1 Merger trees construction

The DM merger trees are constructed internally by GALACTICUS. Inside this merger trees, DM halos (and subhalos) are placed.

The selected algorithm is a minor modification of the original algorithm developed by Cole et al. (2000). The original algorithm splits the halo mass M_1 into two masses, M_2 and M_3. The first mass determined is M_2, this mass is determined from the branching distribution function in the range $M_{\rm res}$ to $\frac{M_1}{2}$. $M_{\rm res}$ is the resolution mass, then M_3 is determined by

$$M_3 = M_1(1-F) - M_2, \tag{5.2.3}$$

where F is the fraction of the parent halo mass gained through sub-resolution accretion in this timestep. Here, it is possible to observe that the subresolution accretion is removed from the mass M_3 and not from M_2. When M_2 is close to $M_1/2$ an asymmetry is shown in progenitor mass functions close to $M_1/2$.

This is solved by first drawing a mass M_2' from the mass branching distribution function and then defining

$$M_2 = M_2'(1-F), \tag{5.2.4}$$

$$M_3 = (M_1 - M_2')(1-F). \tag{5.2.5}$$

The algorithm requires choosing two parameter values that control the numerical precision of the algorithm.

`mergeProbability=0.1` It is the maximum probability of a binary merger allowed in a single timestep. This allows the probability to be kept small, so that the probability for multiple mergers within a single timestep is small.

`accretionLimit=0.1` The maximum fractional change in mass due to subresolution accretion allowed in any given timestep when building the tree.

This building method requires us to specify the probabilities with DM halos can merge. We chose probabilities calibrated with N-body simulations and constrained with observational data based on the work of Parkinson et al. (2008)

plus an additional term.

$$G\left(\frac{\sigma_1}{\sigma_2}, \frac{\delta_2}{\sigma_2}\right) = G_0 \left(\frac{\sigma_1}{\sigma_2}\right)^{\gamma_1} \left(\frac{\delta_2}{\sigma_2}\right)^{\gamma_2} \left(1 - \frac{\sigma_2^2}{\sigma_1^2}\right)^{\gamma_3}. \tag{5.2.6}$$

In this equation, $\sigma_i = (M_i)$ is the usual present-day, linear-theory mass-variance in spheres enclosing an average mass M, M_2 is the mass of the parent halo, M_1 is the mass of the child halo, and δ_2 is the critical overdensity for collapse at the epoch of the parent. The values of the best match with observations are the following:

$$\begin{aligned} G_0 &= +1.14254683789855, \\ \gamma_1 &= -0.327359703026759, \\ \gamma_2 &= +0.0587448775510245, \\ \gamma_3 &= +0.645617093475741. \end{aligned}$$

Finally, we need to specify the $z = 0$ masses of the trees and how many trees to create. We select a uniform distribution of tree masses with masses between $3.0 \cdot 10^9 - 1.1 \cdot 10^{15}\ M_\odot$. We also specify TREESPERDECADE=384. This is the number of trees per decade of halo mass to generate. Finally, the sample rate of the halo mass is given by a power law:

$$\gamma(M) = \log_{10} M/M_{\text{Minimum}}{}^{-\frac{\alpha}{\alpha+1}}, \tag{5.2.7}$$

with $\alpha = 1$, and $M_{\text{Minimum}} = 3.0 \cdot 10^9\ M_\odot$.

5.3 Free parameters summary

Our model has free parameters that need to be fixed.

- A_{res} : Appears in equation 4.1.1, and regulates the amount of gas which is transferred to the NSC gas reservoir.
- a : The free parameter in the mass distribution.
- $\epsilon_\bullet$: The free parameter which regulates the fraction of stellar mass of the NSC converted into a seed.
- ϵ_r: We introduce an efficiency parameter to use a fraction of the radius of the NSC to compute the critical mass.

The next Section describes the models used to fix the parameters mentioned above.

Chapter 6

Analysis

In this chapter, we describe the models run and analyze the respective results of the simulations.

6.1 Estimating the value of $A_{\rm res}$

To estimate the value of $A_{\rm res}$ we compare the nuclear star cluster mass function predicted by GALACTICUS as function of $A_{\rm res}$ with the one observed in the Local Universe.

Originally, Antonini et al. (2015) reported the value of $A_{\rm res} \approx 10^{-3} - 10^{-2}$. In order to calibrate the NSC mass function, we explored different values for $A_{\rm res}$ close to the previously reported. Initial values are given in Table 6.1.1.

Model	$A_{\rm res}$	Resolution $[M_\odot]$
A	$1 \cdot 10^{-4}$	$4.86 \cdot 10^7$
B	$5 \cdot 10^{-3}$	$4.86 \cdot 10^7$
C	$1 \cdot 10^{-2}$	$4.86 \cdot 10^7$
D	$5 \cdot 10^{-2}$	$4.86 \cdot 10^7$
E	$1 \cdot 10^{-1}$	$4.86 \cdot 10^7$

Table 6.1.1: Values of $A_{\rm res}$ for models A, B, C, D and E in GALACTICUS. All the simulations use an equal mass resolution.

From comparing with the observed mass function in Figure 6.1.1, model A decreases from $\Phi_{\rm NSC} = 10^{-1}$ Mpc^{-3} dex^{-1} to $\Phi_{\rm NSC} = 10^{-5}$ Mpc^{-3} dex^{-1} faster

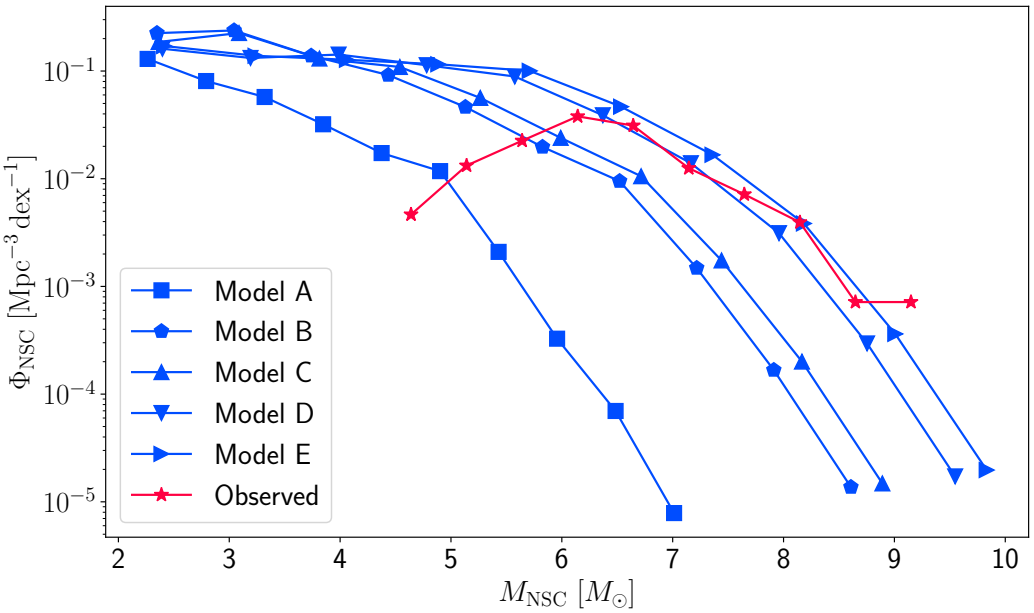

Figure 6.1.1: Nuclear star cluster mass function for different values of $A_{\rm res}$ (solid blue lines) indicated in Table 6.1.1. The observed NSC mass function (solid pink line) is constructed using the available data from Neumayer et al. (2020). All models show a clear tendency to decrease the population as the mass of the NSCs increases. This figure corresponds to the output of GALACTICUS at $z = 0$. Note that the x-axis corresponds to the dynamical mass of the NSC.

than other models and predicts a maximum NSC mass close to 10^7 $M_\odot$. Consequently, model A underestimates the observed population of NSCs.

Models B and C decrease from $\Phi_{\rm NSC} = 10^{-1}$ Mpc^{-3} dex^{-1} to $\Phi_{\rm NSC} = 10^{-5}$ Mpc^{-3} dex^{-1} but with NSC masses from 10^2 $M_\odot$ to $\sim$ 10^9 $M_\odot$. Both models still underestimate the observed population of NSCs at masses higher than 10^6 $M_\odot$. However, the maximum masses predicted are close to 10^9 $M_\odot$, which is in agreement with the observations.

On the other hand, models D and E maintain the predicted population of NSCs approximately constant at $\Phi_{\rm NSC} \sim 10^{-1}$ Mpc^{-3} dex^{-1} for NSCs with masses between $10^2 - 10^6$ $M_\odot$ and reach NSC masses up to 10^{10} $M_\odot$. These models fit well with the observed mass function in the range of $10^6 - 10^9$ $M_\odot$ but predict masses larger than we observe. For models D and E, the overestimation in the population occurs in masses below 10^7 $M_\odot$. This could be due to the mass resolution of the simulation.

We choose $A_{\rm res} = 1 \cdot 10^{-2}$ (model C) as the best fit value for the parameter $A_{\rm res}$.

This is consistent with the value reported by Antonini et al. (2015) to calibrate their in-situ NSC formation scenario.

6.2 Resolution

Once the value of $A_{\rm res}$ is fixed, we explore the effect of mass resolution in our simulations. The values adopted to explore a range of resolutions are given in Table 6.2.1.

line Model	$A_{\rm res}$	Resolution $[M_\odot]$
F	$1 \cdot 10^{-2}$	$4.86 \cdot 10^{7}$
G	$1 \cdot 10^{-2}$	$4.86 \cdot 10^{8}$
H	$1 \cdot 10^{-2}$	$4.86 \cdot 10^{9}$
I	$1 \cdot 10^{-2}$	$4.86 \cdot 10^{10}$

Table 6.2.1: Values of the mass resolution for models F, G, H and I. The value of $A_{\rm res}$ is fixed and set equal to $1 \cdot 10^{-2}$ in all models.

We explore different values for the mass resolution ranging from $4.86 \cdot 10^7\, M_\odot$ to $4.86 \cdot 10^{10}\, M_\odot$. The values used are tentative to study the general behavior of the mass function under changes in resolution.

In figure 6.2.1, all the models predict different values for the NSC population with masses between $10^3 - 10^5\ M_\odot$ and show an abrupt decrease from $\Phi_{\rm NSC} \sim 10^{-2}\,{\rm Mpc}^{-3}\,{\rm dex}^{-1}$ to $\Phi_{\rm NSC} \sim 10^{-5}\,{\rm Mpc}^{-3}\,{\rm dex}^{-1}$ in the mass function at $\sim 10^7\ M_\odot$.

Models F and G show similar behaviors, both models start with $\Phi_{\rm NSC} \sim 10^{-1}\ {\rm Mpc}^{-3}\,{\rm dex}^{-1}$ at $M_{\rm NSC} = 10^2\ M_\odot$ and maintain the line approximately constant until they decrease from $M_{\rm NSC} = 10^5\ M_\odot$ to $M_{\rm NSC} \sim 10^9\ M_\odot$. Models H and I show a completely different tendency; Model H predicts $\Phi_{\rm NSC} = 10^{-2}\,{\rm Mpc}^{-3}\,{\rm dex}^{-1}$ at $M_{\rm NSC} = 10^2\ M_\odot$, increases the value of $\Phi_{\rm NSC}$ until it reaches a peak ($\Phi_{\rm NSC} \sim 10^{-1}\ {\rm Mpc}^{-3}\,{\rm dex}^{-1}$) in $M_{\rm NSC} \sim 10^{4.5}\ M_\odot$ and then decreases to $\Phi_{\rm NSC} \sim 10^{-5}\ {\rm Mpc}^{-3}\,{\rm dex}^{-1}$. Model I starts from $\Phi_{\rm NSC} = 10^{-4}\ {\rm Mpc}^{-3}\,{\rm dex}^{-1}$ at $M_{\rm NSC} = 10^2\ M_\odot$, grows to $\Phi_{\rm NSC} \sim 10^{-2}\ {\rm Mpc}^{-3}\,{\rm dex}^{-1}$ in NSCs with masses between $10^6 - 10^7$ and then decreases until it reaches $\Phi_{\rm NSC} = 10^{-5}\ {\rm Mpc}^{-3}\,{\rm dex}^{-1}$. Model I is the only one comparable to the observed NSC mass function, but

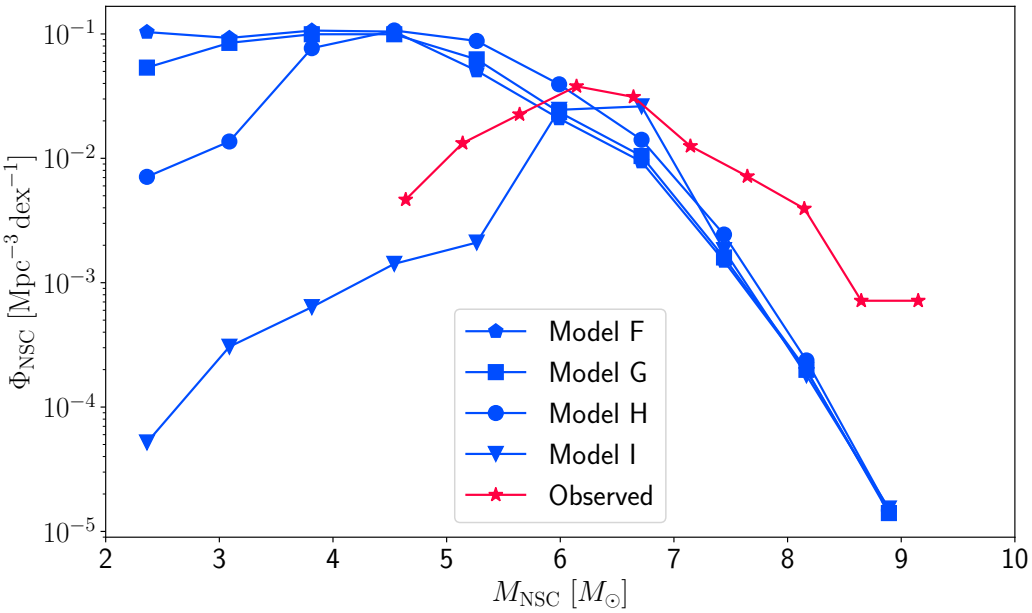

Figure 6.2.1: NSC mass function (solid blue lines) for the different models indicated in Table 6.2.1. The solid pink line corresponds to the observed mass function. This corresponds to the output of GALACTICUS at $z = 0$. The x-axis shows the dynamical mass of the NSC.

underestimates the mass function in NSCs with a mass in the range of $\sim 10^{4.5} - 10^{6}\ M_\odot$.

We explore mass resolutions close to $4.86 \cdot 10^{10}\ M_\odot$ (model I) to analyze the convergence of the mass resolution in the neighborhood. The Table 6.2.2 shows the resolution values for models close to model I.

Model	$A_{\rm res}$	Resolution [$M_\odot$]
J	$1 \cdot 10^{-2}$	$9.0 \cdot 10^{9}$
K	$1 \cdot 10^{-2}$	$1.0 \cdot 10^{10}$
L	$1 \cdot 10^{-2}$	$2.0 \cdot 10^{10}$
M	$1 \cdot 10^{-2}$	$3.0 \cdot 10^{10}$
N	$1 \cdot 10^{-2}$	$4.86 \cdot 10^{10}$

Table 6.2.2: Values of the resolution for $A_{\rm res} = 1 \cdot 10^{-2}$ in the vicinity $4.86 \cdot 10^{10}\ M_\odot$ resolution.

From figure 6.2.2 it is possible to note that all models overlap in the range of $10^{7} - 10^{9}\ M_\odot$, while the order of magnitude of the NSC mass function is different in the low mass regimen ($10^{2} - 10^{6}\ M_\odot$). Models J and K are similar to each

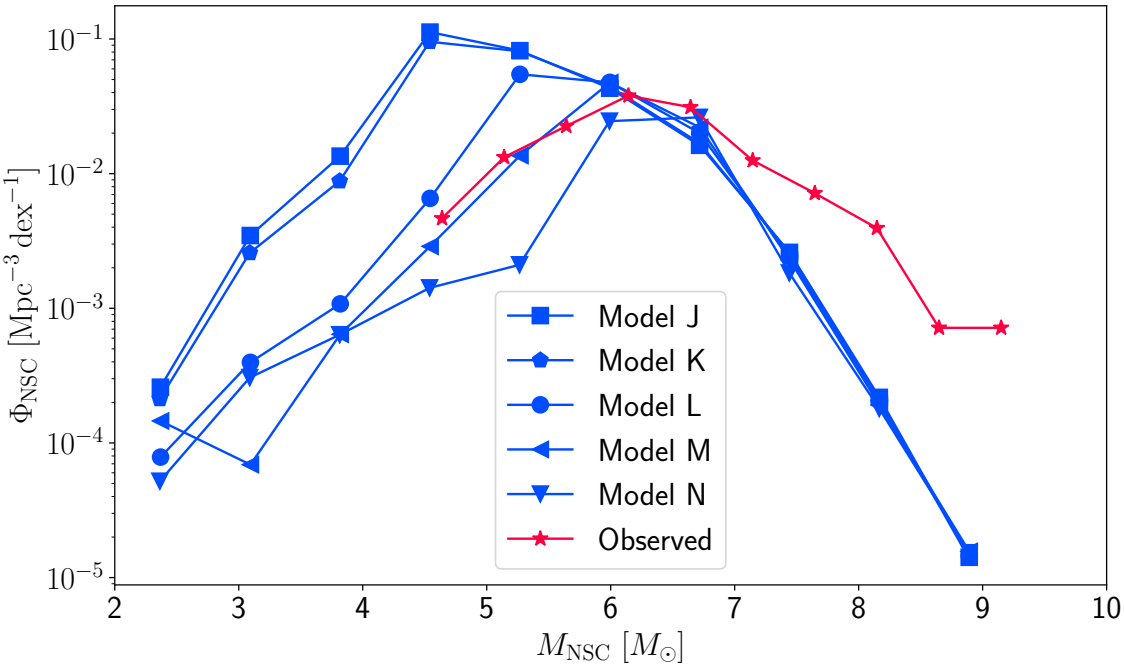

Figure 6.2.2: NSC mass function for different values of the mass resolution in the vecinity of $4.86 \cdot 10^{10}$ $M_\odot$ resolution . The models are indicated in table 6.2.2 compared with the observed NSC mass function. This corresponds to the output of GALACTICUS at $z = 0$.

other; both start at $\Phi_{\rm NSC} \sim 10^{-4}$ Mpc^{-3} dex^{-1} at $M_{\rm NSC} = 10^2$ $M_\odot$, reach a peak at $\Phi_{\rm NSC} = 10^{-1}$ Mpc^{-3} dex^{-1} in NSCs with mass $\sim 10^{4.5}$ $M_\odot$ and then decay. Models L, M, and N have similar behaviors but reach a peak at different masses; model L has the peak ($\Phi_{\rm NSC} \sim 5 \cdot 10^{-2}$ Mpc^{-3} dex^{-1}) at $M_{\rm NSC} = 10^5$ $M_\odot$, model M reaches the peak ($\Phi_{\rm NSC} \sim 10^{-2}$ Mpc^{-3} dex^{-1}) at $M_{\rm NSC} = 10^6$ $M_\odot$, while model N has the maximum value ($\Phi_{\rm NSC} \sim 10^{-2}$ Mpc^{-3} dex^{-1}) at $M_{\rm NSC} \sim 10^7$ $M_\odot$.

Model M is the best approximation to the observed mass function in masses below 10^6 $M_\odot$. However, model M correctly predicts the mass function in the range $10^{4.5} - 10^7$ $M_\odot$, but with an underestimate in the NSC population at masses larger than 10^7 $M_\odot$. A possible explanation could be that the mechanism explored in this thesis is not sufficient to reproduce the observed population of NSCs, and more scenarios must be considered to reach a large population of NSCs with higher masses.

On the other hand, the resolution also affects the BH mass function. To observe the effects of the resolution, in figure 6.2.3 we show the comparison with the predicted BH mass function and the observed mass function.

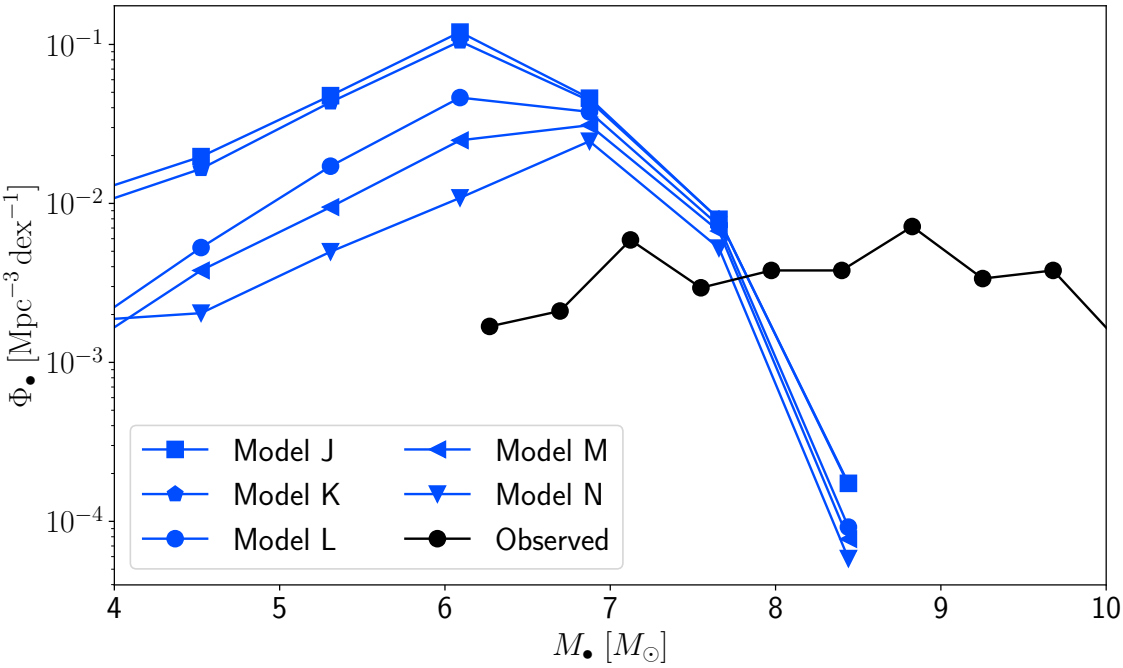

Figure 6.2.3: BH mass function for different values of the mass resolution (solid blue line) in the vecinity of $4.86 \cdot 10^{10}$ $M_\odot$ resolution. The observed BH mass function is constructed with the available data from Kormendy and Ho (2013). The models are indicated in Table 6.2.2. All models converge at a final BH mass $\sim 10^{8.5}$ $M_\odot$. This corresponds to the output of GALACTICUS at $z = 0$.

It is possible to see that all models converge to a maximum mass of $\sim 10^{8.5}\, M_\odot$ and overestimate the BH mass function in masses below $\sim 10^8\, M_\odot$. Although the overestimation ranges from almost one order of magnitude, the shape of the BH mass function does not change abruptly as the resolution varies. Actually, in low masses, all the models increase the value of $\Phi_\bullet$ until they reach a peak and start to decrease. Models J, K, and L begin to decrease at $M_\bullet = 10^6\ M_\odot$, and models M and N start to decrease at $M_\bullet = 10^7\ M_\odot$ where the maximum is reached ($\Phi_\bullet = 10^{-1}$ Mpc^{-3} dex^{-1}). On the other hand, Models M and N start at $\Phi_\bullet \sim 3 \cdot 10^{-3}$ Mpc^{-3} dex^{-1} at $M_\bullet = 10^4\ M_\odot$, grow until the peak ($\Phi_\bullet = 10^{-2}$ Mpc^{-3} dex^{-1}) occurs at $M_\bullet = 10^7\ M_\odot$ and then decrease to $\Phi_\bullet = 10^{-5}$ Mpc^{-3} dex^{-1}.

6.3 Formation of black hole seeds

Each galaxy contains an initial BH seed $M_\bullet = 10\ M_\odot$. In Table 6.3.1, we show the values of ϵ_r used to calculate the critical mass of NSCs. We do not allow NSCs to form in model R. The purpose of this restriction is to compare the mass function of BHs without the contribution of the accreting gas from the NSC gas reservoir and the formation of BH seeds.. We include a lower threshold for the minimum stellar mass that a NSC must contain to form a BH seed. This threshold is introduced to avoid collapse in NSCs with non-physical masses due to the numerical method.

Model	$A_{\rm res}$	Resolution $[M_\odot]$	ϵ_r	$\epsilon_\bullet$	$M_{\rm Threshold}\,[M_\odot]$
O	$1\cdot10^{-2}$	$3.0\cdot10^{10}$	1	0.5	10^3
P	$1\cdot10^{-2}$	$3.0\cdot10^{10}$	0.5	0.5	10^3
Q	$1\cdot10^{-2}$	$3.0\cdot10^{10}$	0.1	0.5	10^3
R	$1\cdot10^{-2}$	$3.0\cdot10^{10}$	-	-	-

Table 6.3.1: Values of the ϵ_r parameter controlling the percentage of the radius of the NSC used to compute the critical mass. Model R does not include gas accretion from the gas reservoir and does not form any seeds from the new included channel. We assume that the efficiency formation of the seed is $\epsilon_\bullet = 0.5$ as this value is the maximum efficiency reached in Vergara et al. (2023).

In figure 6.3.1, we show the mass function of NSCs (solid blue lines) compared to the mass function of the critical masses (dashed purple lines) for each model mentioned in table 6.3.1.

All NSC mass functions overlap and there is no considerable change due to the formation of seeds; Models O, P, and Q predict $\Phi_{\rm NSC} = 10^{-4}\ {\rm Mpc}^{-3}\,{\rm dex}^{-1}$ at $M_{\rm NSC} \sim 10^3\ M_\odot$, increase the value of $\Phi_{\rm NSC}$ until they reach a peak ($\Phi_{\rm NSC} \sim 5\cdot10^{-2}\ {\rm Mpc}^{-3}\,{\rm dex}^{-1}$) at $M_{\rm NSC} \sim 10^6\ M_\odot$ and then decrease. The behavior of the critical mass distributions is similar, but a decrease in the value of $\epsilon_{\rm r}$ moves the distribution to the left; the critical mass distribution of model O has a behavior similar to the NSC mass functions, reaching a peak $10^6\ M_\odot$ but also shows critical masses higher than predicted by the model and observed. Models P and Q have peaks in $\sim 10^{7.8}\,M_\odot$ and $\sim 10^{8.5}\,M_\odot$, respectively, but with similar values in $\Phi_{\rm NSC} \sim 5\cdot10^{-2}\ {\rm Mpc}^{-3}\,{\rm dex}^{-1}$. Models P and Q predict critical masses larger than the NSC masses, which means that NSCs are very stable to form a BH seed in these models.

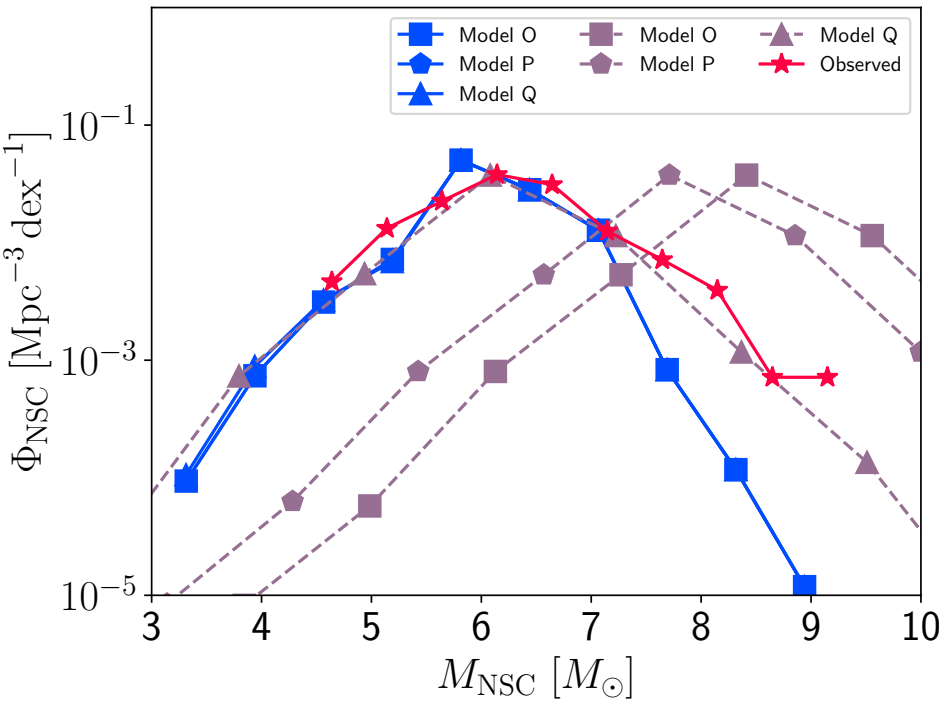

Figure 6.3.1: NSC mass function (solid blue lines) for galaxies containing NSC with dynamical masses larger than 10^3 $M_\odot$. We include the critical mass function for each model (dashed purple lines) and the observed NSC mass function (solid pink line).

Figure 6.3.2 shows the BH mass function predicted by Galacticus. Comparison between each model shows that the distribution does not change considerably with the inclusion of the new model. While models O, P, and Q start with $\Phi_\bullet \sim 10^{-3}$ Mpc^{-3} dex^{-1} at $M_\bullet = 10^4$ $M_\odot$, grow to $\Phi_\bullet \sim 3 \cdot 10^{-2}$ Mpc^{-3} dex^{-1} at $M_\bullet \sim 10^{6.9}$ $M_\odot$ and then decrease to $\Phi_\bullet \sim 3 \cdot 10^{-4}$ Mpc^{-3} dex^{-1} at $M_\bullet = 10^{8.5}$ $M_\odot$, the model R maintains the population of BHs approximately constant ($\Phi_\bullet \sim 10^{-2}$ Mpc^{-3} dex^{-1} in BH masses between $10^4 - 10^6$ $M_\odot$), increases a negligible amount and then decreases. The main change is the increase in the maximum mass predicted by Galacticus and the tendency to decrease the predicted BH population as the mass of the BH decreases.

A possible explanation for the lower masses reached could be the late formation of the seeds, resulting in short timescales to accrete the material and merge with other SMBHs. Although there is an increase in the final mass, the increment is less than one order of magnitude.

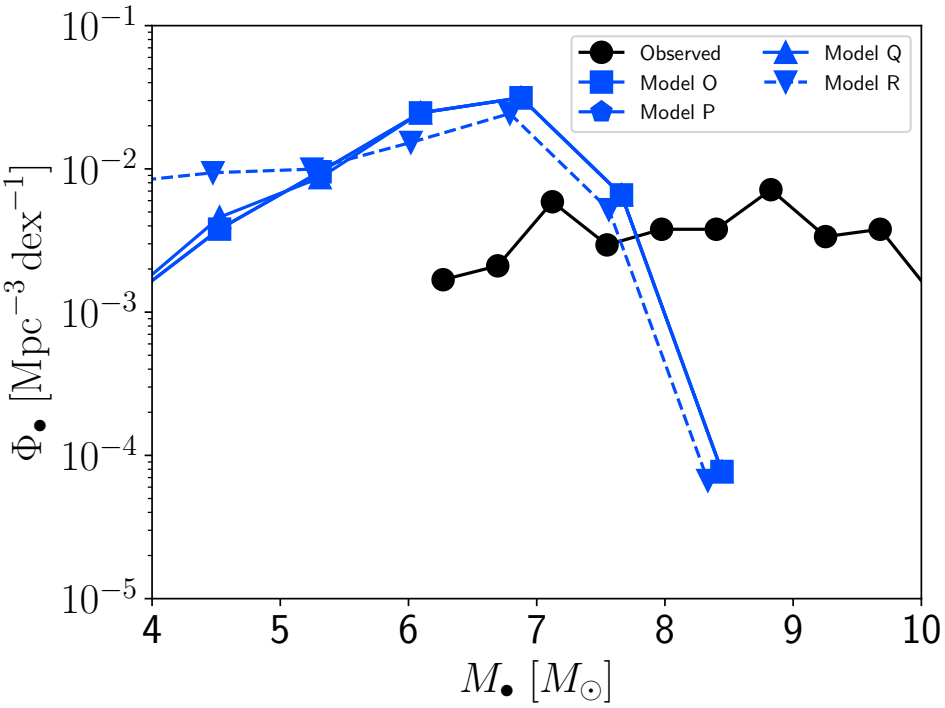

Figure 6.3.2: BH mass function (solid blue lines) for galaxies containing a BH with masses larger than 10^4 $M_\odot$. We include the observed mass function constructed with the available data in Kormendy and Ho (2013).

6.4 Properties of collapsed NSCs

We explore the properties of collapsing NSCs by extracting relevant information at the collapse moment. We extract the stellar mass, critical mass, velocity, and radius of the NSCs.

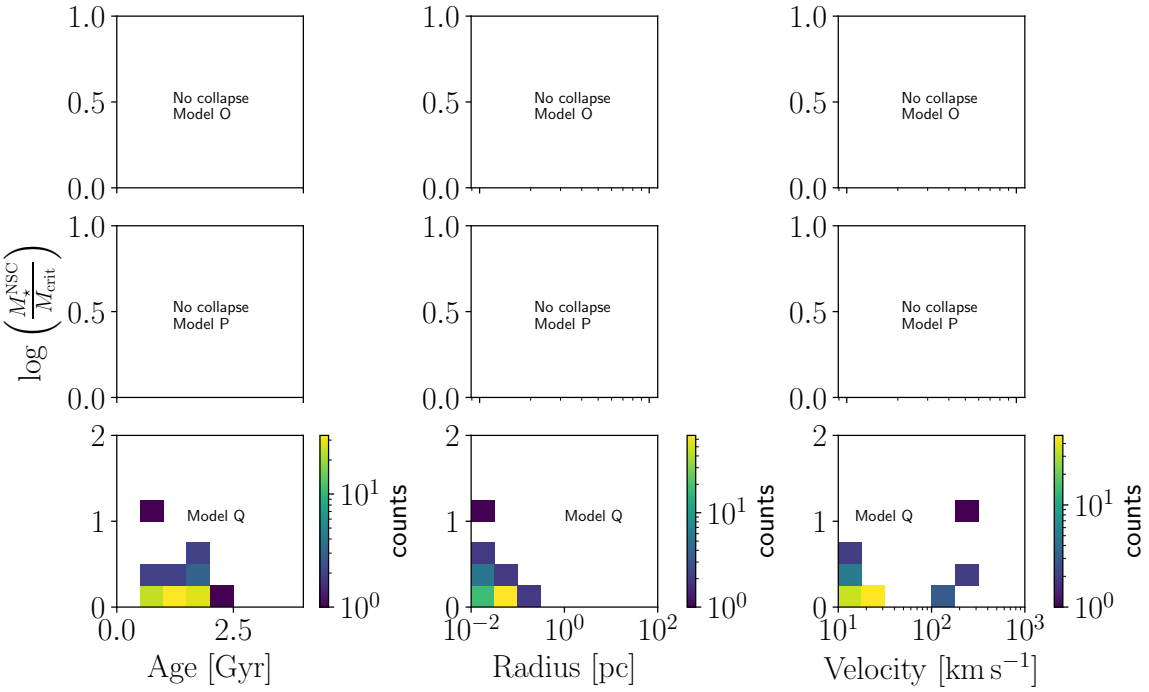

Figure 6.4.1: Properties of the NSC at the moment of collapse. In the y-axis is the stellar mass of the NSC normalized by the critical mass. In the x axis is the age (in Gyr), radius (pc) and the velocity (km s^{-1}), from left to right, respectively. The age and the radius distribution of the NSCs are restricted to 0.8 Gyr to 2.1 Gyr and 0.01 pc to 0.11 pc, respectively. The velocity distribution shows a different behavior and takes values on the order of 10 km s^{-1} and 10^2 km s^{-1}. The colorbar indicates the number of NSCs collapsing per bin.

From the figure 6.4.1, it is straightforward to observe that model O and P do not form BH seeds. Model Q is the only model where the conditions to form a BH seed are fulfilled. In this model, the ages of the NSCs are restricted to values ranging from 0.8 Gyr to 2.1 Gyr. Similarly, the radius of the NSCs ranges from 0.01 pc to 0.11 pc, while the velocity takes different values on the order of 10 km s^{-1} and 10^2 km s^{-1}.

From the figure 6.4.2, it is possible to see that the number of BH seeds decreases as the mass of the BH increases. This means that the model is efficient in forming light seeds (in the order of $10^3\ M_\odot$), but it does not exclude the formation of heavy

seeds up to $10^5\,M_\odot$.

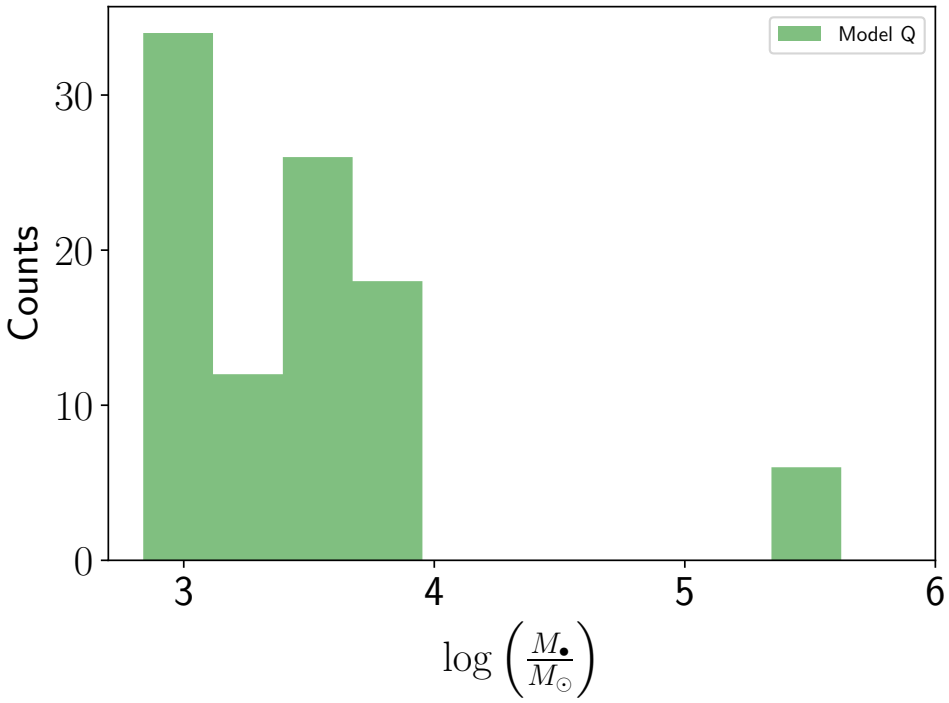

Figure 6.4.2: Mass distribution of the formed BH seeds by model Q. The peak of the distribution occurs at $M_\bullet = 10^3\,M_\odot$, where 35 BH seeds were formed. The most massive formed seeds reach masses $\sim 10^{5.5}\,M_\odot$. There is a gap in the mass distribution.

In summary, model Q shows that the formation of BH seeds inside NSCs is possible, but with a strong dependence on the radius in the critical mass. The model predicts an efficient formation of light seeds ($\sim 10^3\,M_\odot$) but does not exclude the formation of heavy seeds with masses on the order of $\sim 10^{5.5}\,M_\odot$.

Chapter 7

Conclusions and future work

7.1 Conclusions

We have implemented an in situ NSC formation and evolution model in Galacticus and have calibrated the NSC mass function to the observed using the available data from Neumayer et al. (2020).

We find that our value of $A_{\rm res} = 1 \cdot 10^{-2}$ is in the range previously reported by Antonini et al. (2015). A higher value of $A_{\rm res}$ results in larger NSC masses than observed. We also find that our best match models underestimate the number density of NSCs with dynamical masses larger than 10^7 $M_\odot$. This could be explained due to the lack of another formation mechanism (e.g., globular cluster migration).

The results of our simulations strongly depend on the resolution. To reproduce the observed NSC mass function, we decreased the mass resolution, resolving just the most massive DM halos. This is relevant because the in situ star formation scenario is related to more massive halos and galaxies, where the time scale from migration of globular cluster from the disk to the center is too large to contribute to the final mass of the NSC. However, the overestimation of NSCs with dynamical masses less than $\sim 10^6$ $M_\odot$ when the resolution is increased (that means that we resolve less massive DM halos) could be due to our spatial resolution limits in telescopes when they observe the center of galaxies.

We find that at the moment of collapse, all the NSCs in model Q have a similar

radius; ranging from 0.01 pc to 0.11 pc, and the age of the NSCs is also restricted to values between 0.8 Gyr and 2.1 Gyr. The velocity of NSCs shows an interesting behavior, while the majority of NSCs collapse with velocities of the order of $10\,\mathrm{km\,s^{-1}}$, there are a few clusters that collapse at velocities of the order of $10^2\,\mathrm{km\,s^{-1}}$. This might occur in dense clusters, where the core of the cluster encloses more stars and the collision rate timescale increases.

The inclusion of this new scenario of BH formation increases the final mass reached in the BH mass function predicted by Galacticus, but it is still not sufficient to reach masses higher than $10^{8.5}\ M_\odot$. This could be due to the late formation of the BH seeds. According to our simulations, the collapse occurs when the universe is $2-6$ years old. This corresponds to $z\sim 3$ to $z\sim 1$, which implies that BHs have a short time to grow and reach larger masses.

7.2 Future work

The following steps are to explore more parameters related to BH growth, for example, the temperature of the gas that feeds the BH and the value of $\epsilon_\bullet$. Furthermore, the inclusion of a tidal disruption of the stars of the NSCs when they move close to the BH or the inclusion of more formation scenarios could help to calibrate the BH mass function at $z=0$. Inclusion of more scenarios could form early BH seeds that will have more time to grow from accretion and mergers, and reach larger masses at $z=0$.

Once the model is calibrated at $z=0$, we plan to construct the BH mass function at high redshifts. This will allow us to make predictions for gravitational wave emissions from the merge of BHs with intermediate masses for the Laser Interferometer Space Antenna (LISA). LISA is expected to detect the emission of gravitational waves from BH binaries, and according to Barausse et al. (2023), a crucial aspect of the model for predicting the emission of the gravitational waves is the initial mass function of the black hole seeds at high redshift. With the model calibrated, we will be able to make predictions for the gravitational waves emitted by the mergers of the BHs formed under this scenario.

However, for the local universe, we expect the Extremely Large Telescope (ELT) equipped with the Multi-AO Imaging Camera for Deep Observations (MICADO) to resolve the dynamics of dense stellar systems and black holes in near galaxies.

This is due to the point-source sensitivity comparable to the James Webb Space Telescope and a resolution of about a factor 6 better (Davies et al., 2018). This will facilitate the measurement of proper motions in dense NSCs that could host (or not) a BH. Actually, this problem arises with the slope of the $M_{\rm BH} - \sigma$ relation. In elliptical galaxies and classical bulges of disk galaxies, the first estimate was $M_{\rm BH} \propto \sigma^4$ (Tremaine et al., 2002), but recently the relation was adjusted to $M_{\rm BH} \propto \sigma^{5.6}$ (McConnell and Ma, 2013). The slope of the relation is different for globular clusters and the hosted BH. The work of Lützgendorf et al. (2013) found that the relation is $M_{\rm BH} \propto \sigma^{2.3}$, which implies that the slope is defined by different formation processes.

With the MICADO instrument, the possibility of resolving the proper motions of NSCs in the local universe is open. It will be interesting to analyze any anisotropy that could imply the existence of a massive object at their center. From figure 6.4.2 we would expect to observe at least BHs with masses $\gtrsim 10^5\ M_\odot$ inside the NSCs in the local universe.

The ELT/MICADO and the JWST telescope will increase the observational sample of NSCs and BHs. Due to the improvement in the spatial resolution of the telescopes, it is expected to reduce the error bars in the BH and NSC mass estimation and, in consequence, reduce the errors in the scaling relations between their properties, which will give us insights about their origins.

Bibliography

Agarwal, M. and Milosavljević, M. (2011). Nuclear star clusters from clustered star formation. *The Astrophysical Journal*, 729(1):35.

Antonini, F., Barausse, E., and Silk, J. (2015). The coevolution of nuclear star clusters, massive black holes, and their host galaxies. *The Astrophysical Journal*, 812(1):72.

Arons, J. and Silk, J. (1968). On the Jean's criterion in relativistic cosmology. *MNRAS*, 140:331.

Balcells, M., Graham, A. W., and Peletier, R. F. (2007). Galactic Bulges from Hubble Space Telescope NICMOS Observations: Global Scaling Relations. *ApJ*, 665(2):1104–1114.

Bañados, E., Venemans, B., Decarli, R., Farina, E., Mazzucchelli, C., Walter, F., Fan, X., Stern, D., Schlafly, E., Chambers, K., et al. (2016). The pan-starrs1 distant z> 5.6 quasar survey: more than 100 quasars within the first gyr of the universe. *The Astrophysical Journal Supplement Series*, 227(1):11.

Barausse, E. (2012). The evolution of massive black holes and their spins in their galactic hosts. *Monthly Notices of the Royal Astronomical Society*, 423(3):2533–2557.

Barausse, E., Dey, K., Crisostomi, M., Panayada, A., Marsat, S., and Basak, S. (2023). Implications of the pulsar timing array detections for massive black hole mergers in the LISA band. *PHYSICAL REVIEW D*, 108(10):103034.

Bekki, K. (2007). The formation of stellar galactic nuclei through dissipative gas dynamics. *Publications of the Astronomical Society of Australia*, 24(2):77–94.

Bekki, K., Couch, W. J., and Shioya, Y. (2006). Dissipative transformation of nonnucleated dwarf galaxies into nucleated systems. *The Astrophysical Journal*, 642(2):L133.

Belokurov, V., Zucker, D. B., Evans, N. W., Gilmore, G., Vidrih, S., Bramich, D. M., Newberg, H. J., Wyse, R. F. G., Irwin, M. J., Fellhauer, M., Hewett, P. C., Walton, N. A., Wilkinson, M. I., Cole, N., Yanny, B., Rockosi, C. M., Beers, T. C., Bell, E. F., Brinkmann, J., Ivezić, Ž., and Lupton, R. (2006). The Field of Streams: Sagittarius and Its Siblings. *ApJ*, 642(2):L137–L140.

Benson, A. J. (2010). Galaxy formation theory. *Physics Reports*, 495(2):33–86.

Benson, A. J. (2012). Galacticus: A semi-analytic model of galaxy formation. *New Astronomy*, 17(2):175–197.

Benson, A. J., Bower, R. G., Frenk, C. S., Lacey, C. G., Baugh, C. M., and Cole, S. (2003). What Shapes the Luminosity Function of Galaxies? *ApJ*, 599(1):38–49.

Benson, A. J., Cole, S., Frenk, C. S., Baugh, C. M., and Lacey, C. G. (2000). The nature of galaxy bias and clustering. *MNRAS*, 311(4):793–808.

Berlind, A. A. and Weinberg, D. H. (2002). The Halo Occupation Distribution: Toward an Empirical Determination of the Relation between Galaxies and Mass. *ApJ*, 575(2):587–616.

Bertone, G., Hooper, D., and Silk, J. (2005). Particle dark matter: evidence, candidates and constraints. *Phys. Rep.*, 405(5-6):279–390.

Bett, P., Eke, V., Frenk, C. S., Jenkins, A., Helly, J., and Navarro, J. (2007). The spin and shape of dark matter haloes in the Millennium simulation of a Λ cold dark matter universe. *MNRAS*, 376(1):215–232.

Binney, J. and Tremaine, S. (2008). Galactic dynamics. princeton, nj, princeton university press, 2008, 747 p.

Blumenthal, G. R., Faber, S. M., Primack, J. R., and Rees, M. J. (1984). Formation of galaxies and large-scale structure with cold dark matter. *Nature*, 311:517–525.

Böker, T., Laine, S., van der Marel, R. P., Sarzi, M., Rix, H.-W., Ho, L. C., and Shields, J. C. (2002). A hubble space telescope census of nuclear star clusters in late-type spiral galaxies. i. observations and image analysis. *The Astronomical Journal*, 123(3):1389.

Böker, T., Sarzi, M., McLaughlin, D. E., van der Marel, R. P., Rix, H.-W., Ho, L. C., and Shields, J. C. (2004). A Hubble Space Telescope Census of Nuclear Star Clusters in Late-Type Spiral Galaxies. II. Cluster Sizes and Structural Parameter Correlations. *AJ*, 127(1):105–118.

Bond, J. R., Arnett, W. D., and Carr, B. J. (1984). The evolution and fate of Very Massive Objects. *ApJ*, 280:825–847.

Booth, C. M. and Schaye, J. (2009). Cosmological simulations of the growth of supermassive black holes and feedback from active galactic nuclei: method and tests. *MNRAS*, 398(1):53–74.

Capuzzo-Dolcetta, R. (1993). The evolution of the globular cluster system in a triaxial galaxy: can a galactic nucleus form by globular cluster capture? *The Astrophysical Journal*, 415:616.

Capuzzo-Dolcetta, R. and Mastrobuono-Battisti, A. (2009). Globular cluster system erosion in elliptical galaxies. *Astronomy & Astrophysics*, 507(1):183–193.

Chabrier, G. (2001). The Galactic Disk Mass Budget. I. Stellar Mass Function and Density. *ApJ*, 554(2):1274–1281.

Chabrier, G. (2003). Galactic Stellar and Substellar Initial Mass Function. *PASP*, 115(809):763–795.

Chandrasekhar, S. (1943). Dynamical Friction. I. General Considerations: the Coefficient of Dynamical Friction. *ApJ*, 97:255.

Ciotti, L., Ostriker, J. P., and Proga, D. (2009). Feedback from Central Black Holes in Elliptical Galaxies. I. Models with Either Radiative or Mechanical Feedback but not Both. *ApJ*, 699(1):89–104.

Civano, F., Neumayer, N., and Walcher, C. J. (2012). Are nuclear star clusters the precursors of massive black holes? *Advances in Astronomy*, 2012:709038.

Cole, S., Lacey, C. G., Baugh, C. M., and Frenk, C. S. (2000). Hierarchical galaxy formation. *MNRAS*, 319(1):168–204.

Cora, S. A. (2013). State of the art of semi-analytic models. *Asociacion Argentina de Astronomia La Plata Argentina Book Series*, 4:49.

Côté, P., Piatek, S., Ferrarese, L., Jordán, A., Merritt, D., Peng, E. W., Haşegan, M., Blakeslee, J. P., Mei, S., West, M. J., et al. (2006). The acs virgo cluster survey. viii. the nuclei of early-type galaxies. *The Astrophysical Journal Supplement Series*, 165(1):57.

Croton, D. J., Stevens, A. R. H., Tonini, C., Garel, T., Bernyk, M., Bibiano, A., Hodkinson, L., Mutch, S. J., Poole, G. B., and Shattow, G. M. (2016). Semi-Analytic Galaxy Evolution (SAGE): Model Calibration and Basic Results. *ApJS*, 222(2):22.

Davies, R., Alves, J., Clénet, Y., Lang-Bardl, F., Nicklas, H., Pott, J. U., Ragazzoni, R., Tolstoy, E., Amico, P., Anwand-Heerwart, H., Barboza, S., Barl, L., Baudoz, P., Bender, R., Bezawada, N., Bizenberger, P., Boland, W., Bonifacio, P., Borgo, B., Buey, T., Chapron, F., Chemla, F., Cohen, M., Czoske, O., Déo, V., Disseau, K., Dreizler, S., Dupuis, O., Fabricius, M., Falomo, R., Fedou, P., Förster Schreiber, N., Garrel, V., Geis, N., Gemperlein, H., Gendron, E., Genzel, R., Gillessen, S., Glück, M., Grupp, F., Hartl, M., Häuser, M., Hess, H. J., Hofferbert, R., Hopp, U., Hörmann, V., Hubert, Z., Huby, E., Huet, J. M., Hutterer, V., Ives, D., Janssen, A., Jellema, W., Kausch, W., Kerber, F., Kravcar, H., Le Ruyet, B., Leschinski, K., Mandla, C., Manhart, M., Massari, D., Mei, S., Merlin, F., Mohr, L., Monna, A., Muench, N., Müller, F., Musters, G., Navarro, R., Neumann, U., Neumayer, N., Niebsch, J., Plattner, M., Przybilla, N., Rabien, S., Ramlau, R., Ramos, J., Ramsay, S., Rhode, P., Richter, A., Richter, J., Rix, H. W., Rodeghiero, G., Rohloff, R. R.,

Rosensteiner, M., Rousset, G., Schlichter, J., Schubert, J., Sevin, A., Stuik, R., Sturm, E., Thomas, J., Tromp, N., Verdoes-Kleijn, G., Vidal, F., Wagner, R., Wegner, M., Zeilinger, W., Ziegleder, J., Ziegler, B., and Zins, G. (2018). The MICADO first light imager for the ELT: overview, operation, simulation. In Evans, C. J., Simard, L., and Takami, H., editors, *Ground-based and Airborne Instrumentation for Astronomy VII*, volume 10702 of *Society of Photo-Optical Instrumentation Engineers (SPIE) Conference Series*, page 107021S.

Di Matteo, T., Springel, V., and Hernquist, L. (2005). Energy input from quasars regulates the growth and activity of black holes and their host galaxies. *Nature*, 433(7026):604–607.

Dunkley, J., Komatsu, E., Nolta, M. R., Spergel, D. N., Larson, D., Hinshaw, G., Page, L., Bennett, C. L., Gold, B., Jarosik, N., Weiland, J. L., Halpern, M., Hill, R. S., Kogut, A., Limon, M., Meyer, S. S., Tucker, G. S., Wollack, E., and Wright, E. L. (2009). Five-Year Wilkinson Microwave Anisotropy Probe Observations: Likelihoods and Parameters from the WMAP Data. *ApJS*, 180(2):306–329.

Eckner, C., Hou, X., Serpico, P. D., Winter, M., Zaharijas, G., Martin, P., di Mauro, M., Mirabal, N., Petrovic, J., Prodanovic, T., et al. (2018). Millisecond pulsar origin of the galactic center excess and extended gamma-ray emission from andromeda: a closer look. *The Astrophysical Journal*, 862(1):79.

Edgar, R. (2004). A review of bondi–hoyle–lyttleton accretion. *New Astronomy Reviews*, 48(10):843–859.

Einasto, J. (1965). On the Construction of a Composite Model for the Galaxy and on the Determination of the System of Galactic Parameters. *Trudy Astrofizicheskogo Instituta Alma-Ata*, 5:87–100.

Eisenstein, D. J. and Hu, W. (1999). Power Spectra for Cold Dark Matter and Its Variants. *ApJ*, 511(1):5–15.

Eke, V. R., Cole, S., Frenk, C. S., and Navarro, J. F. (1996). Cluster correlation functions in N-body simulations. *MNRAS*, 281:703.

Emsellem, E., Renaud, F., Bournaud, F., Elmegreen, B., Combes, F., and Gabor, J. M. (2015). The interplay between a galactic bar and a supermassive black hole: nuclear fuelling in a subparsec resolution galaxy simulation. *Monthly Notices of the Royal Astronomical Society*, 446(3):2468–2482.

Emsellem, E. and Van De Ven, G. (2008). Formation of central massive objects via tidal compression. *The Astrophysical Journal*, 674(2):653.

Escala, A. (2021). Observational support for massive black hole formation driven by runaway stellar collisions in galactic nuclei. *The Astrophysical Journal*, 908(1):57.

Event Horizon Telescope Collaboration, Akiyama, K., Alberdi, A., Alef, W., Algaba, J. C., Anantua, R., Asada, K., Azulay, R., Bach, U., Baczko, A.-K.,

Ball, D., Baloković, M., Barrett, J., Bauböck, M., Benson, B. A., Bintley, D., Blackburn, L., Blundell, R., Bouman, K. L., Bower, G. C., Boyce, H., Bremer, M., Brinkerink, C. D., Brissenden, R., Britzen, S., Broderick, A. E., Broguiere, D., Bronzwaer, T., Bustamante, S., Byun, D.-Y., Carlstrom, J. E., Ceccobello, C., Chael, A., Chan, C.-k., Chatterjee, K., Chatterjee, S., Chen, M.-T., Chen, Y., Cheng, X., Cho, I., Christian, P., Conroy, N. S., Conway, J. E., Cordes, J. M., Crawford, T. M., Crew, G. B., Cruz-Osorio, A., Cui, Y., Davelaar, J., De Laurentis, M., Deane, R., Dempsey, J., Desvignes, G., Dexter, J., Dhruv, V., Doeleman, S. S., Dougal, S., Dzib, S. A., Eatough, R. P., Emami, R., Falcke, H., Farah, J., Fish, V. L., Fomalont, E., Ford, H. A., Fraga-Encinas, R., Freeman, W. T., Friberg, P., Fromm, C. M., Fuentes, A., Galison, P., Gammie, C. F., García, R., Gentaz, O., Georgiev, B., Goddi, C., Gold, R., Gómez-Ruiz, A. I., Gómez, J. L., Gu, M., Gurwell, M., Hada, K., Haggard, D., Haworth, K., Hecht, M. H., Hesper, R., Heumann, D., Ho, L. C., Ho, P., Honma, M., Huang, C.-W. L., Huang, L., Hughes, D. H., Ikeda, S., Impellizzeri, C. M. V., Inoue, M., Issaoun, S., James, D. J., Jannuzi, B. T., Janssen, M., Jeter, B., Jiang, W., Jiménez-Rosales, A., Johnson, M. D., Jorstad, S., Joshi, A. V., Jung, T., Karami, M., Karuppusamy, R., Kawashima, T., Keating, G. K., Kettenis, M., Kim, D.-J., Kim, J.-Y., Kim, J., Kim, J., Kino, M., Koay, J. Y., Kocherlakota, P., Kofuji, Y., Koch, P. M., Koyama, S., Kramer, C., Kramer, M., Krichbaum, T. P., Kuo, C.-Y., La Bella, N., Lauer, T. R., Lee, D., Lee, S.-S., Leung, P. K., Levis, A., Li, Z., Lico, R., Lindahl, G., Lindqvist, M., Lisakov, M., Liu, J., Liu, K., Liuzzo, E., Lo, W.-P., Lobanov, A. P., Loinard, L., Lonsdale, C. J., Lu, R.-S., Mao, J., Marchili, N., Markoff, S., Marrone, D. P., Marscher, A. P., Martí-Vidal, I., Matsushita, S., Matthews, L. D., Medeiros, L., Menten, K. M., Michalik, D., Mizuno, I., Mizuno, Y., Moran, J. M., Moriyama, K., Moscibrodzka, M., Müller, C., Mus, A., Musoke, G., Myserlis, I., Nadolski, A., Nagai, H., Nagar, N. M., Nakamura, M., Narayan, R., Narayanan, G., Natarajan, I., Nathanail, A., Fuentes, S. N., Neilsen, J., Neri, R., Ni, C., Noutsos, A., Nowak, M. A., Oh, J., Okino, H., Olivares, H., Ortiz-León, G. N., Oyama, T., Özel, F., Palumbo, D. C. M., Paraschos, G. F., Park, J., Parsons, H., Patel, N., Pen, U.-L., Pesce, D. W., Piétu, V., Plambeck, R., PopStefanija, A., Porth, O., Pötzl, F. M., Prather, B., Preciado-López, J. A., Psaltis, D., Pu, H.-Y., Ramakrishnan, V., Rao, R., Rawlings, M. G., Raymond, A. W., Rezzolla, L., Ricarte, A., Ripperda, B., Roelofs, F., Rogers, A., Ros, E., Romero-Cañizales, C., Roshanineshat, A., Rottmann, H., Roy, A. L., Ruiz, I., Ruszczyk, C., Rygl, K. L. J., Sánchez, S., Sánchez-Argüelles, D., Sánchez-Portal, M., Sasada, M., Satapathy, K., Savolainen, T., Schloerb, F. P., Schonfeld, J., Schuster, K.-F., Shao, L., Shen, Z., Small, D., Sohn, B. W., SooHoo, J., Souccar, K., Sun, H., Tazaki, F., Tetarenko, A. J., Tiede, P., Tilanus, R. P. J., Titus, M., Torne, P., Traianou, E., Trent, T., Trippe, S., Turk, M., van Bemmel, I., van Langevelde, H. J., van Rossum, D. R., Vos, J., Wagner, J., Ward-Thompson, D., Wardle, J., Weintroub, J., Wex, N., Wharton, R., Wielgus, M., Wiik, K., Witzel, G., Wondrak, M. F., Wong, G. N., Wu, Q., Yamaguchi, P., Yoon, D., Young, A., Young, K., Younsi, Z., Yuan, F., Yuan,

Y.-F., Zensus, J. A., Zhang, S., Zhao, G.-Y., Zhao, S.-S., Agurto, C., Allardi, A., Amestica, R., Araneda, J. P., Arriagada, O., Berghuis, J. L., Bertarini, A., Berthold, R., Blanchard, J., Brown, K., Cárdenas, M., Cantzler, M., Caro, P., Castillo-Domínguez, E., Chan, T. L., Chang, C.-C., Chang, D. O., Chang, S.-H., Chang, S.-C., Chen, C.-C., Chilson, R., Chuter, T. C., Ciechanowicz, M., Colin-Beltran, E., Coulson, I. M., Crowley, J., Degenaar, N., Dornbusch, S., Durán, C. A., Everett, W. B., Faber, A., Forster, K., Fuchs, M. M., Gale, D. M., Geertsema, G., González, E., Graham, D., Gueth, F., Halverson, N. W., Han, C.-C., Han, K.-C., Hasegawa, Y., Hernández-Rebollar, J. L., Herrera, C., Herrero-Illana, R., Heyminck, S., Hirota, A., Hoge, J., Hostler Schimpf, S. R., Howie, R. E., Huang, Y.-D., Jiang, H., Jinchi, H., John, D., Kimura, K., Klein, T., Kubo, D., Kuroda, J., Kwon, C., Lacasse, R., Laing, R., Leitch, E. M., Li, C.-T., Liu, C.-T., Liu, K.-Y., Lin, L. C. C., Lu, L.-M., Mac-Auliffe, F., Martin-Cocher, P., Matulonis, C., Maute, J. K., Messias, H., Meyer-Zhao, Z., Montaña, A., Montenegro-Montes, F., Montgomerie, W., Moreno Nolasco, M. E., Muders, D., Nishioka, H., Norton, T. J., Nystrom, G., Ogawa, H., Olivares, R., Oshiro, P., Pérez-Beaupuits, J. P., Parra, R., Phillips, N. M., Poirier, M., Pradel, N., Qiu, R., Raffin, P. A., Rahlin, A. S., Ramírez, J., Ressler, S., Reynolds, M., Rodríguez-Montoya, I., Saez-Madain, A. F., Santana, J., Shaw, P., Shirkey, L. E., Silva, K. M., Snow, W., Sousa, D., Sridharan, T. K., Stahm, W., Stark, A. A., Test, J., Torstensson, K., Venegas, P., Walther, C., Wei, T.-S., White, C., Wieching, G., Wijnands, R., Wouterloot, J. G. A., Yu, C.-Y., Yu, W., and Zeballos, M. (2022). First Sagittarius A* Event Horizon Telescope Results. I. The Shadow of the Supermassive Black Hole in the Center of the Milky Way. *ApJ*, 930(2):L12.

Event Horizon Telescope Collaboration, Akiyama, K., Alberdi, A., Alef, W., Asada, K., Azulay, R., Baczko, A.-K., Ball, D., Baloković, M., Barrett, J., Bintley, D., Blackburn, L., Boland, W., Bouman, K. L., Bower, G. C., Bremer, M., Brinkerink, C. D., Brissenden, R., Britzen, S., Broderick, A. E., Broguiere, D., Bronzwaer, T., Byun, D.-Y., Carlstrom, J. E., Chael, A., Chan, C.-k., Chatterjee, S., Chatterjee, K., Chen, M.-T., Chen, Y., Cho, I., Christian, P., Conway, J. E., Cordes, J. M., Crew, G. B., Cui, Y., Davelaar, J., De Laurentis, M., Deane, R., Dempsey, J., Desvignes, G., Dexter, J., Doeleman, S. S., Eatough, R. P., Falcke, H., Fish, V. L., Fomalont, E., Fraga-Encinas, R., Freeman, W. T., Friberg, P., Fromm, C. M., Gómez, J. L., Galison, P., Gammie, C. F., García, R., Gentaz, O., Georgiev, B., Goddi, C., Gold, R., Gu, M., Gurwell, M., Hada, K., Hecht, M. H., Hesper, R., Ho, L. C., Ho, P., Honma, M., Huang, C.-W. L., Huang, L., Hughes, D. H., Ikeda, S., Inoue, M., Issaoun, S., James, D. J., Jannuzi, B. T., Janssen, M., Jeter, B., Jiang, W., Johnson, M. D., Jorstad, S., Jung, T., Karami, M., Karuppusamy, R., Kawashima, T., Keating, G. K., Kettenis, M., Kim, J.-Y., Kim, J., Kim, J., Kino, M., Koay, J. Y., Koch, P. M., Koyama, S., Kramer, M., Kramer, C., Krichbaum, T. P., Kuo, C.-Y., Lauer, T. R., Lee, S.-S., Li, Y.-R., Li, Z., Lindqvist, M., Liu, K., Liuzzo, E., Lo, W.-P., Lobanov, A. P., Loinard, L., Lonsdale, C., Lu, R.-S., MacDonald, N. R., Mao, J., Markoff, S., Marrone, D. P., Marscher,

A. P., Martí-Vidal, I., Matsushita, S., Matthews, L. D., Medeiros, L., Menten, K. M., Mizuno, Y., Mizuno, I., Moran, J. M., Moriyama, K., Moscibrodzka, M., Müller, C., Nagai, H., Nagar, N. M., Nakamura, M., Narayan, R., Narayanan, G., Natarajan, I., Neri, R., Ni, C., Noutsos, A., Okino, H., Olivares, H., Ortiz-León, G. N., Oyama, T., Özel, F., Palumbo, D. C. M., Patel, N., Pen, U.-L., Pesce, D. W., Piétu, V., Plambeck, R., PopStefanija, A., Porth, O., Prather, B., Preciado-López, J. A., Psaltis, D., Pu, H.-Y., Ramakrishnan, V., Rao, R., Rawlings, M. G., Raymond, A. W., Rezzolla, L., Ripperda, B., Roelofs, F., Rogers, A., Ros, E., Rose, M., Roshanineshat, A., Rottmann, H., Roy, A. L., Ruszczyk, C., Ryan, B. R., Rygl, K. L. J., Sánchez, S., Sánchez-Arguelles, D., Sasada, M., Savolainen, T., Schloerb, F. P., Schuster, K.-F., Shao, L., Shen, Z., Small, D., Sohn, B. W., SooHoo, J., Tazaki, F., Tiede, P., Tilanus, R. P. J., Titus, M., Toma, K., Torne, P., Trent, T., Trippe, S., Tsuda, S., van Bemmel, I., van Langevelde, H. J., van Rossum, D. R., Wagner, J., Wardle, J., Weintroub, J., Wex, N., Wharton, R., Wielgus, M., Wong, G. N., Wu, Q., Young, K., Young, A., Younsi, Z., Yuan, F., Yuan, Y.-F., Zensus, J. A., Zhao, G., Zhao, S.-S., Zhu, Z., Algaba, J.-C., Allardi, A., Amestica, R., Anczarski, J., Bach, U., Baganoff, F. K., Beaudoin, C., Benson, B. A., Berthold, R., Blanchard, J. M., Blundell, R., Bustamente, S., Cappallo, R., Castillo-Domínguez, E., Chang, C.-C., Chang, S.-H., Chang, S.-C., Chen, C.-C., Chilson, R., Chuter, T. C., Córdova Rosado, R., Coulson, I. M., Crawford, T. M., Crowley, J., David, J., Derome, M., Dexter, M., Dornbusch, S., Dudevoir, K. A., Dzib, S. A., Eckart, A., Eckert, C., Erickson, N. R., Everett, W. B., Faber, A., Farah, J. R., Fath, V., Folkers, T. W., Forbes, D. C., Freund, R., Gómez-Ruiz, A. I., Gale, D. M., Gao, F., Geertsema, G., Graham, D. A., Greer, C. H., Grosslein, R., Gueth, F., Haggard, D., Halverson, N. W., Han, C.-C., Han, K.-C., Hao, J., Hasegawa, Y., Henning, J. W., Hernández-Gómez, A., Herrero-Illana, R., Heyminck, S., Hirota, A., Hoge, J., Huang, Y.-D., Impellizzeri, C. M. V., Jiang, H., Kamble, A., Keisler, R., Kimura, K., Kono, Y., Kubo, D., Kuroda, J., Lacasse, R., Laing, R. A., Leitch, E. M., Li, C.-T., Lin, L. C. C., Liu, C.-T., Liu, K.-Y., Lu, L.-M., Marson, R. G., Martin-Cocher, P. L., Massingill, K. D., Matulonis, C., McColl, M. P., McWhirter, S. R., Messias, H., Meyer-Zhao, Z., Michalik, D., Montaña, A., Montgomerie, W., Mora-Klein, M., Muders, D., Nadolski, A., Navarro, S., Neilsen, J., Nguyen, C. H., Nishioka, H., Norton, T., Nowak, M. A., Nystrom, G., Ogawa, H., Oshiro, P., Oyama, T., Parsons, H., Paine, S. N., Peñalver, J., Phillips, N. M., Poirier, M., Pradel, N., Primiani, R. A., Raffin, P. A., Rahlin, A. S., Reiland, G., Risacher, C., Ruiz, I., Sáez-Madaín, A. F., Sassella, R., Schellart, P., Shaw, P., Silva, K. M., Shiokawa, H., Smith, D. R., Snow, W., Souccar, K., Sousa, D., Sridharan, T. K., Srinivasan, R., Stahm, W., Stark, A. A., Story, K., Timmer, S. T., Vertatschitsch, L., Walther, C., Wei, T.-S., Whitehorn, N., Whitney, A. R., Woody, D. P., Wouterloot, J. G. A., Wright, M., Yamaguchi, P., Yu, C.-Y., Zeballos, M., Zhang, S., and Ziurys, L. (2019). First M87 Event Horizon Telescope Results. I. The Shadow of the Supermassive Black Hole. *ApJ*, 875(1):L1.

Fan, X., Bañados, E., and Simcoe, R. A. (2023). Quasars and the Intergalactic

Medium at Cosmic Dawn. *ARA&A*, 61:373–426.

Ferramacho, L. D., Blanchard, A., and Zolnierowski, Y. (2009). Constraints on CDM cosmology from galaxy power spectrum, CMB and SNIa evolution. *A&A*, 499(1):21–29.

Ferrara, A., Salvadori, S., Yue, B., and Schleicher, D. (2014). Initial mass function of intermediate-mass black hole seeds. *MNRAS*, 443(3):2410–2425.

Ferrarese, L., Côté, P., Dalla Bontà, E., Peng, E. W., Merritt, D., Jordán, A., Blakeslee, J. P., Haşegan, M., Mei, S., Piatek, S., et al. (2006). A fundamental relation between compact stellar nuclei, supermassive black holes, and their host galaxies. *The Astrophysical Journal*, 644(1):L21.

Ferrarese, L. and Merritt, D. (2000). A fundamental relation between supermassive black holes and their host galaxies. *The Astrophysical Journal*, 539(1):L9.

Filippenko, A. V. and Ho, L. C. (2003). A low-mass central black hole in the bulgeless seyfert 1 galaxy ngc 4395. *The Astrophysical Journal*, 588(1):L13.

Frenk, C. S. (2002). Simulating the formation of cosmic structure. *Philosophical Transactions of the Royal Society of London Series A*, 360(1795):1277.

Fryer, C. L., Woosley, S. E., and Heger, A. (2001). Pair-Instability Supernovae, Gravity Waves, and Gamma-Ray Transients. *ApJ*, 550(1):372–382.

Fryxell, B., Olson, K., Ricker, P., Timmes, F. X., Zingale, M., Lamb, D. Q., MacNeice, P., Rosner, R., Truran, J. W., and Tufo, H. (2000). FLASH: An Adaptive Mesh Hydrodynamics Code for Modeling Astrophysical Thermonuclear Flashes. *ApJS*, 131(1):273–334.

Gao, L., Navarro, J. F., Cole, S., Frenk, C. S., White, S. D. M., Springel, V., Jenkins, A., and Neto, A. F. (2008). The redshift dependence of the structure of massive Λ cold dark matter haloes. *MNRAS*, 387(2):536–544.

Gao, L., Yoshida, N., Abel, T., Frenk, C. S., Jenkins, A., and Springel, V. (2007). The first generation of stars in the Λ cold dark matter cosmology. *MNRAS*, 378(2):449–468.

Genzel, R., Eisenhauer, F., and Gillessen, S. (2010). The galactic center massive black hole and nuclear star cluster. *Reviews of Modern Physics*, 82(4):3121.

Georgiev, I. Y., Böker, T., Leigh, N., Lützgendorf, N., and Neumayer, N. (2016). Masses and scaling relations for nuclear star clusters, and their co-existence with central black holes. *Monthly Notices of the Royal Astronomical Society*, 457(2):2122–2138.

Ghez, A. M., Salim, S., Weinberg, N. N., Lu, J. R., Do, T., Dunn, J. K., Matthews, K., Morris, M. R., Yelda, S., Becklin, E. E., Kremenek, T., Milosavljevic, M., and Naiman, J. (2008). Measuring Distance and Properties of the Milky Way's Central Supermassive Black Hole with Stellar Orbits. *ApJ*, 689(2):1044–1062.

Gillessen, S., Eisenhauer, F., Fritz, T. K., Bartko, H., Dodds-Eden, K., Pfuhl, O., Ott, T., and Genzel, R. (2009). The Orbit of the Star S2 Around SGR A* from Very Large Telescope and Keck Data. *ApJ*, 707(2):L114–L117.

Ginsburg, A., Goddi, C., Kruijssen, J. M. D., Bally, J., Smith, R., Galván-Madrid, R., Mills, E. A. C., Wang, K., Dale, J. E., Darling, J., Rosolowsky, E., Loughnane, R., Testi, L., and Bastian, N. (2017). Thermal Feedback in the High-mass Star- and Cluster-forming Region W51. *ApJ*, 842(2):92.

Gnedin, N. Y. and Hui, L. (1998). Probing the Universe with the Lyalpha forest - I. Hydrodynamics of the low-density intergalactic medium. *MNRAS*, 296(1):44–55.

Gnedin, O. Y. (2003). Tidal Effects in Clusters of Galaxies. *ApJ*, 582(1):141–161.

Graham, A. W. and Spitler, L. R. (2009). Quantifying the coexistence of massive black holes and dense nuclear star clusters. *Monthly Notices of the Royal Astronomical Society*, 397(4):2148–2162.

Haiman, Z. (2004). Constraints from Gravitational Recoil on the Growth of Supermassive Black Holes at High Redshift. *ApJ*, 613(1):36–40.

Haiman, Z., Ciotti, L., and Ostriker, J. P. (2004). Reasoning from fossils: learning from the local black hole population about the evolution of quasars. *The Astrophysical Journal*, 606(2):763.

Heger, A., Fryer, C. L., Woosley, S. E., Langer, N., and Hartmann, D. H. (2003). How Massive Single Stars End Their Life. *ApJ*, 591(1):288–300.

Heitmann, K., White, M., Wagner, C., Habib, S., and Higdon, D. (2010). The Coyote Universe. I. Precision Determination of the Nonlinear Matter Power Spectrum. *ApJ*, 715(1):104–121.

Henriques, B. M. B., Thomas, P. A., Oliver, S., and Roseboom, I. (2009). Monte Carlo Markov Chain parameter estimation in semi-analytic models of galaxy formation. *MNRAS*, 396(1):535–547.

Hinshaw, G., Larson, D., Komatsu, E., Spergel, D. N., Bennett, C. L., Dunkley, J., Nolta, M. R., Halpern, M., Hill, R. S., Odegard, N., Page, L., Smith, K. M., Weiland, J. L., Gold, B., Jarosik, N., Kogut, A., Limon, M., Meyer, S. S., Tucker, G. S., Wollack, E., and Wright, E. L. (2013). Nine-year Wilkinson Microwave Anisotropy Probe (WMAP) Observations: Cosmological Parameter Results. *ApJS*, 208(2):19.

Hirano, S., Hosokawa, T., Yoshida, N., Umeda, H., Omukai, K., Chiaki, G., and Yorke, H. W. (2014). One Hundred First Stars: Protostellar Evolution and the Final Masses. *ApJ*, 781(2):60.

Hirano, S., Zhu, N., Yoshida, N., Spergel, D., and Yorke, H. W. (2015). Early Structure Formation from Primordial Density Fluctuations with a Blue, Tilted Power Spectrum. *ApJ*, 814(1):18.

Hoyer, N., Neumayer, N., Georgiev, I. Y., Seth, A. C., and Greene, J. E. (2021). The nucleation fraction of local volume galaxies. *MNRAS*, 507(3):3246–3266.

Hoyle, F., Burgers, J., and van De Hulst, H. (1949). Problems of cosmical aerodynamics. *Central Air Documents, Office, Dayton, OH*.

Hubble, E. P. (1929). A spiral nebula as a stellar system, messier 31. *The Astrophysical Journal*, 69.

Hunt, L. K., Combes, F., García-Burillo, S., Schinnerer, E., Krips, M., Baker, A. J., Boone, F., Eckart, A., Léon, S., Neri, R., et al. (2008). Molecular gas in nuclei of galaxies (nuga)-ix. the decoupled bars and gas inflow in ngc 2782. *Astronomy & Astrophysics*, 482(1):133–150.

Inayoshi, K., Visbal, E., and Haiman, Z. (2020). The Assembly of the First Massive Black Holes. *ARA&A*, 58:27–97.

Jiang, C. Y., Jing, Y. P., Faltenbacher, A., Lin, W. P., and Li, C. (2008). A Fitting Formula for the Merger Timescale of Galaxies in Hierarchical Clustering. *ApJ*, 675(2):1095–1105.

Juodžbalis, I., Conselice, C. J., Singh, M., Adams, N., Ormerod, K., Harvey, T., Austin, D., Volonteri, M., Cohen, S. H., Jansen, R. A., Summers, J., Windhorst, R. A., D'Silva, J. C. J., Koekemoer, A. M., Coe, D., Driver, S. P., Frye, B., Grogin, N. A., Marshall, M. A., Nonino, M., Pirzkal, N., Robotham, A., , Russell E. Ryan, J., Ortiz, Rafael, I., Tompkins, S., Willmer, C. N. A., and Yan, H. (2023). EPOCHS VII: discovery of high-redshift ($6.5 < z < 12$) AGN candidates in JWST ERO and PEARLS data. *MNRAS*, 525(1):1353–1364.

Katz, N. and White, S. D. M. (1993). Hierarchical Galaxy Formation: Overmerging and the Formation of an X-Ray Cluster. *ApJ*, 412:455.

Kennicutt, Robert C., J. (1989). The Star Formation Law in Galactic Disks. *ApJ*, 344:685.

Kennicutt, Robert C., J. (1998). The Global Schmidt Law in Star-forming Galaxies. *ApJ*, 498(2):541–552.

Kim, W.-T. and Elmegreen, B. G. (2017). Nuclear spiral shocks and induced gas inflows in weak oval potentials. *The Astrophysical Journal Letters*, 841(1):L4.

King, A. (2015). How big can a black hole grow? *Monthly Notices of the Royal Astronomical Society: Letters*, 456(1):L109–L112.

Klypin, A., Gottlöber, S., Kravtsov, A. V., and Khokhlov, A. M. (1999). Galaxies in N-Body Simulations: Overcoming the Overmerging Problem. *ApJ*, 516(2):530–551.

Klypin, A. A. and Shandarin, S. F. (1983). Three-dimensional numerical model of the formation of large-scale structure in the Universe. *MNRAS*, 204:891–907.

Komatsu, E., Dunkley, J., Nolta, M. R., Bennett, C. L., Gold, B., Hinshaw, G., Jarosik, N., Larson, D., Limon, M., Page, L., Spergel, D. N., Halpern, M., Hill, R. S., Kogut, A., Meyer, S. S., Tucker, G. S., Weiland, J. L., Wollack, E., and Wright, E. L. (2009). Five-Year Wilkinson Microwave Anisotropy Probe Observations: Cosmological Interpretation. *ApJS*, 180(2):330–376.

Komatsu, E., Smith, K. M., Dunkley, J., Bennett, C. L., Gold, B., Hinshaw, G., Jarosik, N., Larson, D., Nolta, M. R., Page, L., Spergel, D. N., Halpern, M., Hill, R. S., Kogut, A., Limon, M., Meyer, S. S., Odegard, N., Tucker, G. S., Weiland, J. L., Wollack, E., and Wright, E. L. (2011). Seven-year Wilkinson Microwave Anisotropy Probe (WMAP) Observations: Cosmological Interpretation. *ApJS*, 192(2):18.

Kormendy, J. (1982). Observations of Galaxy Structure and Dynamics. *Saas-Fee Advanced Course*, 12:115.

Kormendy, J. and Ho, L. C. (2013). Coevolution (or not) of supermassive black holes and host galaxies. *Annual Review of Astronomy and Astrophysics*, 51:511–653.

Kravtsov, A. V., Klypin, A. A., and Khokhlov, A. M. (1997). Adaptive Refinement Tree: A New High-Resolution N-Body Code for Cosmological Simulations. *ApJS*, 111(1):73–94.

Krumholz, M. R. (2012). Star formation in atomic gas. *The Astrophysical Journal*, 759(1):9.

Krumholz, M. R., McKee, C. F., and Tumlinson, J. (2009). The star formation law in atomic and molecular gas. *The Astrophysical Journal*, 699(1):850.

Krumholz, M. R. and Tan, J. C. (2007). Slow Star Formation in Dense Gas: Evidence and Implications. *ApJ*, 654(1):304–315.

Kudritzki, R.-P. and Puls, J. (2000). Winds from Hot Stars. *ARA&A*, 38:613–666.

Kuhlen, M., Diemand, J., Madau, P., and Zemp, M. (2008). The Via Lactea INCITE simulation: galactic dark matter substructure at high resolution. In *Journal of Physics Conference Series*, volume 125 of *Journal of Physics Conference Series*, page 012008.

Landau, L. D. and Lifshitz, E. M. (2013). *Course of theoretical physics*. Elsevier.

Lapi, A., Raimundo, S., Aversa, R., Cai, Z.-Y., Negrello, M., Celotti, A., De Zotti, G., and Danese, L. (2014). The coevolution of supermassive black holes and massive galaxies at high redshift. *The Astrophysical Journal*, 782(2):69.

Latif, M. A. and Schleicher, D. R. G. (2015). The formation of supermassive black holes in rapidly rotating disks. *A&A*, 578:A118.

Latif, M. A., Schleicher, D. R. G., Schmidt, W., and Niemeyer, J. (2013). The Formation of Massive Population III Stars in the Presence of Turbulence. *ApJ*, 772(1):L3.

Lee, M. H. (1993). N-Body Evolution of Dense Clusters of Compact Stars. *ApJ*, 418:147.

Leigh, N., Böker, T., and Knigge, C. (2012). Nuclear star clusters and the stellar spheroids of their host galaxies. *Monthly Notices of the Royal Astronomical Society*, 424(3):2130–2138.

Li, Y., Haiman, Z., and Mac Low, M.-M. (2007). Correlations between central massive objects and their host galaxies: from bulgeless spirals to ellipticals. *The Astrophysical Journal*, 663(1):61.

Light, E., Danielson, R., and Schwarzschild, M. (1974). The nucleus of m31. *The Astrophysical Journal*, 194:257–263.

Lotz, J. M., Telford, R., Ferguson, H. C., Miller, B. W., Stiavelli, M., and Mack, J. (2001). Dynamical friction in de globular cluster systems. *The Astrophysical Journal*, 552(2):572.

Lucas, W. E., Bonnell, I. A., and Dale, J. E. (2020). Supernova feedback and the energy deposition in molecular clouds. *MNRAS*, 493(4):4700–4710.

Lützgendorf, N., Kissler-Patig, M., Neumayer, N., Baumgardt, H., Noyola, E., de Zeeuw, P. T., Gebhardt, K., Jalali, B., and Feldmeier, A. (2013). M - σrelation for intermediate-mass black holes in globular clusters. *A&A*, 555:A26.

Lynden-Bell, D. (1967). Statistical mechanics of violent relaxation in stellar systems. *MNRAS*, 136:101.

Lyubenova, M., van den Bosch, R. C. E., Côté, P., Kuntschner, H., van de Ven, G., Ferrarese, L., Jordán, A., Infante, L., and Peng, E. W. (2013). The complex nature of the nuclear star cluster in fcc 277. *Monthly Notices of the Royal Astronomical Society*, 431(4):3364–3372.

Maciejewski, W. (2004). Nuclear spirals in galaxies: gas response to an asymmetric potential–ii. hydrodynamical models. *Monthly Notices of the Royal Astronomical Society*, 354(3):892–904.

Mao, S., Mo, H. J., and White, S. D. M. (1998). The evolution of galactic discs. *MNRAS*, 297(3):L71–L75.

Mastropietro, C., Moore, B., Mayer, L., Debattista, V. P., Piffaretti, R., and Stadel, J. (2005a). Morphological evolution of discs in clusters. *MNRAS*, 364(2):607–619.

Mastropietro, C., Moore, B., Mayer, L., Wadsley, J., and Stadel, J. (2005b). The gravitational and hydrodynamical interaction between the Large Magellanic Cloud and the Galaxy. *MNRAS*, 363(2):509–520.

Mayall, N. and Aller, L. (1942). The rotation of the spiral nebula messier 33. *Astrophysical Journal, vol. 95, p. 5*, 95:5.

Mayer, L., Governato, F., Colpi, M., Moore, B., Quinn, T., Wadsley, J., Stadel, J., and Lake, G. (2001a). The Metamorphosis of Tidally Stirred Dwarf Galaxies. *ApJ*, 559(2):754–784.

Mayer, L., Governato, F., Colpi, M., Moore, B., Quinn, T., Wadsley, J., Stadel, J., and Lake, G. (2001b). Tidal Stirring and the Origin of Dwarf Spheroidals in the Local Group. *ApJ*, 547(2):L123–L127.

McConnell, N. J. and Ma, C.-P. (2013). Revisiting the Scaling Relations of Black Hole Masses and Host Galaxy Properties. *ApJ*, 764(2):184.

Miller, M. C. and Hamilton, D. P. (2002). Production of intermediate-mass black holes in globular clusters. *MNRAS*, 330(1):232–240.

Milosavljević, M. (2004). On the origin of nuclear star clusters in late-type spiral galaxies. *The Astrophysical Journal*, 605(1):L13.

Mo, H. J., Mao, S., and White, S. D. M. (1998). The formation of galactic discs. *MNRAS*, 295(2):319–336.

Moore, B., Ghigna, S., Governato, F., Lake, G., Quinn, T., Stadel, J., and Tozzi, P. (1999). Dark Matter Substructure within Galactic Halos. *ApJ*, 524(1):L19–L22.

Moore, B., Katz, N., Lake, G., Dressler, A., and Oemler, A. (1996). Galaxy harassment and the evolution of clusters of galaxies. *Nature*, 379(6566):613–616.

Moore, B., Lake, G., and Katz, N. (1998). Morphological Transformation from Galaxy Harassment. *ApJ*, 495(1):139–151.

Moran, E. C., Shahinyan, K., Sugarman, H. R., Vélez, D. O., and Eracleous, M. (2014). Black Holes At the Centers of Nearby Dwarf Galaxies. *AJ*, 148(6):136.

Narlikar, J. V. and Padmanabhan, T. (2001). Standard Cosmology and Alternatives: A Critical Appraisal. *ARA&A*, 39:211–248.

Natarajan, P. and Treister, E. (2009). Is there an upper limit to black hole masses? *Monthly Notices of the Royal Astronomical Society*, 393(3):838–845.

Navarro, J. F., Frenk, C. S., and White, S. D. M. (1996). The Structure of Cold Dark Matter Halos. *ApJ*, 462:563.

Navarro, J. F., Frenk, C. S., and White, S. D. M. (1997). A Universal Density Profile from Hierarchical Clustering. *ApJ*, 490(2):493–508.

Neistein, E. and Dekel, A. (2008). Constructing merger trees that mimic N-body simulations. *MNRAS*, 383(2):615–626.

Neumayer, N., Seth, A., and Böker, T. (2020). Nuclear star clusters. *The Astronomy and Astrophysics Review*, 28:1–75.

Neumayer, N., Walcher, C. J., Andersen, D., Sánchez, S. F., Böker, T., and Rix, H.-W. (2011). Two-dimensional hα kinematics of bulgeless disc galaxies. *Monthly Notices of the Royal Astronomical Society*, 413(3):1875–1888.

Nguyen, D. D., Seth, A. C., Neumayer, N., Iguchi, S., Cappellari, M., Strader, J., Chomiuk, L., Tremou, E., Pacucci, F., Nakanishi, K., Bahramian, A., Nguyen, P. M., den Brok, M., Ahn, C. C., Voggel, K. T., Kacharov, N., Tsukui, T., Ly, C. K., Dumont, A., and Pechetti, R. (2019). Improved dynamical constraints on the masses of the central black holes in nearby low-mass early-type galactic nuclei and the first black hole determination for ngc 205. *The Astrophysical Journal*, 872(1):104.

Oh, K. and Lin, D. (2000). Nucleation of dwarf galaxies in the virgo cluster. *The Astrophysical Journal*, 543(2):620.

Pacucci, F., Natarajan, P., and Ferrara, A. (2017). Feedback limits to maximum seed masses of black holes. *The Astrophysical Journal Letters*, 835(2):L36.

Parkinson, H., Cole, S., and Helly, J. (2008). Generating dark matter halo merger trees. *MNRAS*, 383(2):557–564.

Pechetti, R., Seth, A., Neumayer, N., Georgiev, I., Kacharov, N., and den Brok, M. (2020). Luminosity Models and Density Profiles for Nuclear Star Clusters for a Nearby Volume-limited Sample of 29 Galaxies. *ApJ*, 900(1):32.

Peebles, P. J. E. (1969). Origin of the Angular Momentum of Galaxies. *ApJ*, 155:393.

Percival, W. J. (2005). Cosmological structure formation in a homogeneous dark energy background. *A&A*, 443(3):819–830.

Percival, W. J., Nichol, R. C., Eisenstein, D. J., Frieman, J. A., Fukugita, M., Loveday, J., Pope, A. C., Schneider, D. P., Szalay, A. S., Tegmark, M., Vogeley, M. S., Weinberg, D. H., Zehavi, I., Bahcall, N. A., Brinkmann, J., Connolly, A. J., and Meiksin, A. (2007a). The Shape of the Sloan Digital Sky Survey Data Release 5 Galaxy Power Spectrum. *ApJ*, 657(2):645–663.

Percival, W. J., Nichol, R. C., Eisenstein, D. J., Weinberg, D. H., Fukugita, M., Pope, A. C., Schneider, D. P., Szalay, A. S., Vogeley, M. S., Zehavi, I., Bahcall, N. A., Brinkmann, J., Connolly, A. J., Loveday, J., and Meiksin, A. (2007b). Measuring the Matter Density Using Baryon Oscillations in the SDSS. *ApJ*, 657(1):51–55.

Planck Collaboration, Akrami, Y., Arroja, F., Ashdown, M., Aumont, J., Baccigalupi, C., Ballardini, M., Banday, A. J., Barreiro, R. B., Bartolo, N., Basak, S., Benabed, K., Bernard, J. P., Bersanelli, M., Bielewicz, P., Bock, J. J., Bond, J. R., Borrill, J., Bouchet, F. R., Boulanger, F., Bucher, M., Burigana, C., Butler, R. C., Calabrese, E., Cardoso, J. F., Carron, J., Challinor, A., Chiang, H. C., Colombo, L. P. L., Combet, C., Contreras, D., Crill, B. P., Cuttaia, F., de Bernardis, P., de Zotti, G., Delabrouille, J., Delouis, J. M.,

Di Valentino, E., Diego, J. M., Donzelli, S., Doré, O., Douspis, M., Ducout, A., Dupac, X., Dusini, S., Efstathiou, G., Elsner, F., Enßlin, T. A., Eriksen, H. K., Fantaye, Y., Fergusson, J., Fernandez-Cobos, R., Finelli, F., Forastieri, F., Frailis, M., Franceschi, E., Frolov, A., Galeotta, S., Galli, S., Ganga, K., Gauthier, C., Génova-Santos, R. T., Gerbino, M., Ghosh, T., González-Nuevo, J., Górski, K. M., Gratton, S., Gruppuso, A., Gudmundsson, J. E., Hamann, J., Handley, W., Hansen, F. K., Herranz, D., Hivon, E., Hooper, D. C., Huang, Z., Jaffe, A. H., Jones, W. C., Keihänen, E., Keskitalo, R., Kiiveri, K., Kim, J., Kisner, T. S., Krachmalnicoff, N., Kunz, M., Kurki-Suonio, H., Lagache, G., Lamarre, J. M., Lasenby, A., Lattanzi, M., Lawrence, C. R., Le Jeune, M., Lesgourgues, J., Levrier, F., Lewis, A., Liguori, M., Lilje, P. B., Lindholm, V., López-Caniego, M., Lubin, P. M., Ma, Y. Z., Macías-Pérez, J. F., Maggio, G., Maino, D., Mandolesi, N., Mangilli, A., Marcos-Caballero, A., Maris, M., Martin, P. G., Martínez-González, E., Matarrese, S., Mauri, N., McEwen, J. D., Meerburg, P. D., Meinhold, P. R., Melchiorri, A., Mennella, A., Migliaccio, M., Mitra, S., Miville-Deschênes, M. A., Molinari, D., Moneti, A., Montier, L., Morgante, G., Moss, A., Münchmeyer, M., Natoli, P., Nørgaard-Nielsen, H. U., Pagano, L., Paoletti, D., Partridge, B., Patanchon, G., Peiris, H. V., Perrotta, F., Pettorino, V., Piacentini, F., Polastri, L., Polenta, G., Puget, J. L., Rachen, J. P., Reinecke, M., Remazeilles, M., Renzi, A., Rocha, G., Rosset, C., Roudier, G., Rubiño-Martín, J. A., Ruiz-Granados, B., Salvati, L., Sandri, M., Savelainen, M., Scott, D., Shellard, E. P. S., Shiraishi, M., Sirignano, C., Sirri, G., Spencer, L. D., Sunyaev, R., Suur-Uski, A. S., Tauber, J. A., Tavagnacco, D., Tenti, M., Toffolatti, L., Tomasi, M., Trombetti, T., Valiviita, J., Van Tent, B., Vielva, P., Villa, F., Vittorio, N., Wandelt, B. D., Wehus, I. K., White, S. D. M., Zacchei, A., Zibin, J. P., and Zonca, A. (2020). Planck 2018 results. X. Constraints on inflation. *A&A*, 641:A10.

Plewa, T. and Müller, E. (2001). AMRA: An Adaptive Mesh Refinement hydrodynamic code for astrophysics. *Computer Physics Communications*, 138(2):101–127.

Portegies Zwart, S. F. and McMillan, S. L. W. (2002). The Runaway Growth of Intermediate-Mass Black Holes in Dense Star Clusters. *ApJ*, 576(2):899–907.

Press, W. H. and Schechter, P. (1974). Formation of Galaxies and Clusters of Galaxies by Self-Similar Gravitational Condensation. *ApJ*, 187:425–438.

Quilis, V. (2004). A new multidimensional adaptive mesh refinement hydro + gravity cosmological code. *MNRAS*, 352(4):1426–1438.

Redman, R. and Shirley, E. (1937). Photometry of the andromeda nebula, m 31'. *Monthly Notices of the Royal Astronomical Society*, 97:416.

Rees, M. J. (1984). Black Hole Models for Active Galactic Nuclei. *ARA&A*, 22:471–506.

Regan, J. A. and Downes, T. P. (2018). Fragmentation inside atomic cooling haloes exposed to Lyman-Werner radiation. *MNRAS*, 475(4):4636–4647.

Reinoso, B., Schleicher, D. R. G., Fellhauer, M., Klessen, R. S., and Boekholt, T. C. N. (2018). Collisions in primordial star clusters. Formation pathway for intermediate mass black holes. *A&A*, 614:A14.

Reinoso, B., Schleicher, D. R. G., Fellhauer, M., Leigh, N. W. C., and Klessen, R. S. (2020). The effects of a background potential in star cluster evolution. A delay in the relaxation time-scale and runaway collision processes. *A&A*, 639:A92.

Rezzolla, L., Barausse, E., Dorband, E. N., Pollney, D., Reisswig, C., Seiler, J., and Husa, S. (2008). Final spin from the coalescence of two black holes. 78(4):044002.

Ricker, P. M., Dodelson, S., and Lamb, D. Q. (2000). COSMOS: A Hybrid N-Body/Hydrodynamics Code for Cosmological Problems. *ApJ*, 536(1):122–143.

Riess, A. G., Rodney, S. A., Scolnic, D. M., Shafer, D. L., Strolger, L.-G., Ferguson, H. C., Postman, M., Graur, O., Maoz, D., Jha, S. W., Mobasher, B., Casertano, S., Hayden, B., Molino, A., Hjorth, J., Garnavich, P. M., Jones, D. O., Kirshner, R. P., Koekemoer, A. M., Grogin, N. A., Brammer, G., Hemmati, S., Dickinson, M., Challis, P. M., Wolff, S., Clubb, K. I., Filippenko, A. V., Nayyeri, H., U, V., Koo, D. C., Faber, S. M., Kocevski, D., Bradley, L., and Coe, D. (2018). Type Ia Supernova Distances at Redshift >1.5 from the Hubble Space Telescope Multi-cycle Treasury Programs: The Early Expansion Rate. *ApJ*, 853(2):126.

Salpeter, E. E. (1964). Accretion of Interstellar Matter by Massive Objects. *ApJ*, 140:796–800.

Sánchez, A. G., Crocce, M., Cabré, A., Baugh, C. M., and Gaztañaga, E. (2009). Cosmological parameter constraints from SDSS luminous red galaxies: a new treatment of large-scale clustering. *MNRAS*, 400(3):1643–1664.

Sanders, R. H. (1970). The Effects of Stellar Collisions in Dense Stellar Systems. *ApJ*, 162:791.

Schinnerer, E., Böker, T., Emsellem, E., and Downes, D. (2007). Bar-driven mass build-up within the central 50 pc of ngc 6946. *Astronomy & Astrophysics*, 462(3):L27–L30.

Schinnerer, E., Böker, T., Emsellem, E., and Lisenfeld, U. (2006). Molecular gas dynamics in ngc 6946: a bar-driven nuclear starburst caught in the act. *The Astrophysical Journal*, 649(1):181.

Schmidt, M. (1959). The Rate of Star Formation. *ApJ*, 129:243.

Seljak, U., Makarov, A., McDonald, P., Anderson, S. F., Bahcall, N. A., Brinkmann, J., Burles, S., Cen, R., Doi, M., Gunn, J. E., Ivezić, Ž., Kent, S., Loveday, J., Lupton, R. H., Munn, J. A., Nichol, R. C., Ostriker, J. P., Schlegel, D. J., Schneider, D. P., Tegmark, M., Berk, D. E., Weinberg, D. H., and York, D. G. (2005). Cosmological parameter analysis including SDSS Lyα

forest and galaxy bias: Constraints on the primordial spectrum of fluctuations, neutrino mass, and dark energy. *Phys. Rev. D*, 71(10):103515.

Sesana, A., Barausse, E., Dotti, M., and Rossi, E. M. (2014). Linking the spin evolution of massive black holes to galaxy kinematics. *The Astrophysical Journal*, 794(2):104.

Seth, A., Agüeros, M., Lee, D., and Basu-Zych, A. (2008). The coincidence of nuclear star clusters and active galactic nuclei. *The Astrophysical Journal*, 678(1):116.

Seth, A. C., Dalcanton, J. J., Hodge, P. W., and Debattista, V. P. (2006). Clues to nuclear star cluster formation from edge-on spirals. *The Astronomical Journal*, 132(6):2539.

Sheth, R. K., Mo, H. J., and Tormen, G. (2001). Ellipsoidal collapse and an improved model for the number and spatial distribution of dark matter haloes. *MNRAS*, 323(1):1–12.

Shlosman, I., Begelman, M. C., and Frank, J. (1990). The fuelling of active galactic nuclei. *Nature*, 345:679–686.

Shu, F. H. (1991). *The Physics of Astrophysics: Gas Dynamics*, volume 2. University Science Books.

Sijacki, D., Springel, V., Di Matteo, T., and Hernquist, L. (2007). A unified model for AGN feedback in cosmological simulations of structure formation. *MNRAS*, 380(3):877–900.

Sijacki, D., Springel, V., and Haehnelt, M. G. (2010). Growing Supermassive Black Holes in Cosmological Simulations of Structure Formation. In Peterson, B. M., Somerville, R. S., and Storchi-Bergmann, T., editors, *Co-Evolution of Central Black Holes and Galaxies*, volume 267, pages 445–450.

Singh, J., Monaco, P., and Tan, J. C. (2023). The formation of supermassive black holes from Population III.1 seeds. II. Evolution to the local universe. *MNRAS*, 525(1):969–982.

Springel, V. (2005). The cosmological simulation code GADGET-2. *MNRAS*, 364(4):1105–1134.

Springel, V., Di Matteo, T., and Hernquist, L. (2005a). Modelling feedback from stars and black holes in galaxy mergers. *MNRAS*, 361(3):776–794.

Springel, V., Wang, J., Vogelsberger, M., Ludlow, A., Jenkins, A., Helmi, A., Navarro, J. F., Frenk, C. S., and White, S. D. M. (2008). The Aquarius Project: the subhaloes of galactic haloes. *MNRAS*, 391(4):1685–1711.

Springel, V., White, S. D. M., Jenkins, A., Frenk, C. S., Yoshida, N., Gao, L., Navarro, J., Thacker, R., Croton, D., Helly, J., Peacock, J. A., Cole, S., Thomas, P., Couchman, H., Evrard, A., Colberg, J., and Pearce, F. (2005b).

Simulations of the formation, evolution and clustering of galaxies and quasars. *Nature*, 435(7042):629–636.

Summers, F. J., Davis, M., and Evrard, A. E. (1995). Galaxy Tracers and Velocity Bias. *ApJ*, 454:1.

Tegmark, M., Blanton, M. R., Strauss, M. A., Hoyle, F., Schlegel, D., Scoccimarro, R., Vogeley, M. S., Weinberg, D. H., Zehavi, I., Berlind, A., Budavari, T., Connolly, A., Eisenstein, D. J., Finkbeiner, D., Frieman, J. A., Gunn, J. E., Hamilton, A. J. S., Hui, L., Jain, B., Johnston, D., Kent, S., Lin, H., Nakajima, R., Nichol, R. C., Ostriker, J. P., Pope, A., Scranton, R., Seljak, U., Sheth, R. K., Stebbins, A., Szalay, A. S., Szapudi, I., Verde, L., Xu, Y., Annis, J., Bahcall, N. A., Brinkmann, J., Burles, S., Castander, F. J., Csabai, I., Loveday, J., Doi, M., Fukugita, M., Gott, J. Richard, I., Hennessy, G., Hogg, D. W., Ivezić, Ž., Knapp, G. R., Lamb, D. Q., Lee, B. C., Lupton, R. H., McKay, T. A., Kunszt, P., Munn, J. A., O'Connell, L., Peoples, J., Pier, J. R., Richmond, M., Rockosi, C., Schneider, D. P., Stoughton, C., Tucker, D. L., Vanden Berk, D. E., Yanny, B., York, D. G., and SDSS Collaboration (2004). The Three-Dimensional Power Spectrum of Galaxies from the Sloan Digital Sky Survey. *ApJ*, 606(2):702–740.

Tegmark, M., Silk, J., Rees, M. J., Blanchard, A., Abel, T., and Palla, F. (1997). How Small Were the First Cosmological Objects? *ApJ*, 474:1.

Tinker, J., Kravtsov, A. V., Klypin, A., Abazajian, K., Warren, M., Yepes, G., Gottlöber, S., and Holz, D. E. (2008). Toward a Halo Mass Function for Precision Cosmology: The Limits of Universality. *ApJ*, 688(2):709–728.

Tormen, G., Diaferio, A., and Syer, D. (1998). Survival of substructure within dark matter haloes. *MNRAS*, 299(3):728–742.

Tremaine, S., Gebhardt, K., Bender, R., Bower, G., Dressler, A., Faber, S. M., Filippenko, A. V., Green, R., Grillmair, C., Ho, L. C., et al. (2002). The slope of the black hole mass versus velocity dispersion correlation. *The Astrophysical Journal*, 574(2):740.

Tremaine, S., Henon, M., and Lynden-Bell, D. (1986). H-functions and mixing in violent relaxation. *MNRAS*, 219:285–297.

Tremaine, S. D., Ostriker, J., and Spitzer Jr, L. (1975). The formation of the nuclei of galaxies. i-m31. *The Astrophysical Journal*, 196:407–411.

Turner, M. L., Côté, P., Ferrarese, L., Jordán, A., Blakeslee, J. P., Mei, S., Peng, E. W., and West, M. J. (2012). The acs fornax cluster survey. vi. the nuclei of early-type galaxies in the fornax cluster. *The Astrophysical Journal Supplement Series*, 203(1):5.

Vergara, M. C., Escala, A., Schleicher, D. R. G., and Reinoso, B. (2023). Global instability by runaway collisions in nuclear stellar clusters: numerical tests of a route for massive black hole formation. *MNRAS*, 522(3):4224–4237.

Villalobos, Á., De Lucia, G., Weinmann, S. M., Borgani, S., and Murante, G. (2013). An improved prescription for merger time-scales from controlled simulations. *MNRAS*, 433(1):L49–L53.

Volonteri, M. (2010). Formation of supermassive black holes. *The Astronomy and Astrophysics Review*, 18:279–315.

Volonteri, M. and Rees, M. J. (2005). Rapid Growth of High-Redshift Black Holes. *ApJ*, 633(2):624–629.

Walcher, C. J., Böker, T., Charlot, S., Ho, L. C., Rix, H. W., Rossa, J., Shields, J. C., and van der Marel, R. P. (2006). Stellar Populations in the Nuclei of Late-Type Spiral Galaxies. *ApJ*, 649(2):692–708.

Wehner, E. H. and Harris, W. E. (2006). From supermassive black holes to dwarf elliptical nuclei: a mass continuum. *The Astrophysical Journal*, 644(1):L17.

Whalen, D. J. and Fryer, C. L. (2012). The Formation of Supermassive Black Holes from Low-mass Pop III Seeds. *ApJ*, 756(1):L19.

White, S. D. M. and Frenk, C. S. (1991). Galaxy Formation through Hierarchical Clustering. *ApJ*, 379:52.

Woods, T. E., Agarwal, B., Bromm, V., Bunker, A., Chen, K.-J., Chon, S., Ferrara, A., Glover, S. C. O., Haemmerlé, L., Haiman, Z., Hartwig, T., Heger, A., Hirano, S., Hosokawa, T., Inayoshi, K., Klessen, R. S., Kobayashi, C., Koliopanos, F., Latif, M. A., Li, Y., Mayer, L., Mezcua, M., Natarajan, P., Pacucci, F., Rees, M. J., Regan, J. A., Sakurai, Y., Salvadori, S., Schneider, R., Surace, M., Tanaka, T. L., Whalen, D. J., and Yoshida, N. (2019). Titans of the early Universe: The Prato statement on the origin of the first supermassive black holes. 36:e027.

Zel'dovich, Y. B. (1964). The Fate of a Star and the Evolution of Gravitational Energy Upon Accretion. *Soviet Physics Doklady*, 9:195.

Zhang, W., Woosley, S. E., and Heger, A. (2008). Fallback and Black Hole Production in Massive Stars. *ApJ*, 679(1):639–654.